ADA037247

DNA 4119F

A SIMPLIFIED MODEL OF SHOCK-ON-SHOCK INTERACTION

Martin Marietta Aerospace
Sand Lake Road
Orlando, Florida 32805

September 1976

Final Report for Period February 1976 – September 1976
CONTRACT No. DNA001-76-C-0175

This work sponsored by the Defense Nuclear Agency under RDT&E RMSS Code B342076464 N99QAXAE50005 H2590D

Approved for public release; distribution unlimited.

Prepared for

Headquarters
DEFENSE NUCLEAR AGENCY (SPAS)
Washington, D.C. 20305

UNCLASSIFIED

SECURITY CLASSIFICATION OF THIS PAGE (When Data Entered)

REPORT DOCUMENTATION PAGE		READ INSTRUCTIONS BEFORE COMPLETING FORM
1. REPORT NUMBER 19 18 DNA 4190F	2. GOVT ACCESSION NO.	3. RECIPIENT'S CATALOG NUMBER
4. TITLE (and Subtitle) 6 A Simplified Model of Shock-on-Shock Interaction.		5. TYPE OF REPORT & PERIOD COVERED 9 Final Report. (DRAFT) Feb[redacted] 30 1976
		6. ~~PERFORMING ORG.~~ REPORT NUMBER 14 OR-14,282 — 30 Sep 76
7. AUTHOR(s) 10 G. F. Aiello		8. CONTRACT OR GRANT NUMBER(s) 15 DNA 001-76-C-0175
9. PERFORMING ORGANIZATION NAME AND ADDRESS Martin Marietta Corporation Post Office Box 5837 Orlando, Florida 32805		10. PROGRAM ELEMENT, PROJECT, TASK AREA & WORK UNIT NUMBERS
11. CONTROLLING OFFICE NAME AND ADDRESS Director Defense Nuclear Agency Washington, D. C. 20305		12. REPORT DATE 11 Aug[redacted]76
		13. NUMBER OF PAGES 76 12 66p.
14. MONITORING AGENCY NAME & ADDRESS (if different from Controlling Office)		15. SECURITY CLASS. (of this report) Unclassified
		15a. DECLASSIFICATION/DOWNGRADING SCHEDULE

16. DISTRIBUTION STATEMENT (of this Report)

Approved for public release; distribution unlimited.

17. DISTRIBUTION STATEMENT (of the abstract entered in Block 20, if different from Report)

18. SUPPLEMENTARY NOTES

This work sponsored by the Defense Nuclear Agency under RDT&E RMSS Code B342076464 N99QAXAE50005 H2590D.

403 238

19. KEY WORDS (Continue on reverse side if necessary and identify by block number)

Blast	Experiment Test
Shock	Hypersonic
Sled Test	Cone
Pressure	

20. ABSTRACT (Continue on reverse side if necessary and identify by block number)

A simplified model is presented of the shock-on-shock problem as it pertains to the encounter between a supersonic cone and a planar blast wave. The model provides an accurate and inexpensive means of predicting the circumferential distribution of peak pressures and pulse duration for all encounter angles between nose-on and broadside with the cone at zero or small angles of attack

DD FORM 1 JAN 73 1473 EDITION OF 1 NOV 65 IS OBSOLETE

UNCLASSIFIED

SECURITY CLASSIFICATION OF THIS PAGE (When Data Entered)

SUMMARY

The shock-on-shock phenomenon represents a potentially dangerous environment to high performance strategic interceptors. Therefore, there is a need to have the capability to predict the pressure distribution history due to such encounters. The objective of this program was to develop a computerized model which is inexpensive to operate as well as accurate. The knowledge required to simplify the model is derived from the Defense Nuclear Agency sled test data and the NASA Ames rigorous analytical results.

The model presented here permits prediction of the circumferential distribution of peak pressures that result from an encounter at any angle from nose-on to broadside. The sharp supersonic conical body may also be at a small (less than the cone half-angle) angle of attack. The model also allows prediction of the circumferential distribution of the duration of the shock-on-shock pulse which is defined as the time it takes for the surface pressure to reach the "quasi-steady" pressure level associated with complete engulfment of the vehicle. Finally, the model permits estimating the engulfment time of a particular axial station of the vehicle, i.e., the time interval between the arrival of the wave front at the subject station on the windward side of the cone and the arrival at that station on the leeward side.

Comparisons between the new model and the existing data show good agreement and, where no comparisons are possible, the new results are plausible. In spite of the simplifying assumptions and some empiricism, the model is expected to be effective over a fairly large range of blast and vehicle conditions except for angle of attack. When the angle of attack increases to the point of flow separation on the leeside of the cone, the model no longer applies; it could, however, be modified to do so.

PREFACE

This final report discusses the "Development of a Simplified Model of Shock-on-Shock Interaction" effort conducted by Martin Marietta Aerospace Orlando Division, under Contract DNA001-76-C-0175, for the Defense Nuclear Agency, Washington, D.C. The reporting period is from February 1976 to September 1976.

The author wishes to acknowledge the vigorous interest and support of Capt. David Garrison who is the Contract Officer Representative for the Defense Nuclear Agency.

In addition, an expression of gratitude is given to Dr. Paul Kutler of NASA Ames and Dr. Leonidas Sakell of Martin Marietta for providing the predictions made with the Ames three-dimensional shock-on-shock interaction solution.

The author also wishes to acknowledge the effort of Mr. Dean Cole of KAMAN Nuclear for providing the digitized sled test data used in this study.

CONTENTS

1.0 Introduction 5

2.0 The Problem - A Function of Encounter Angle 7

3.0 Shock-on-Shock Model 11

3.1 Peak Windward Pressure 12

3.2 Peak Leeward Pressure 19

3.3 Windward Pulse Duration 24

3.4 Leeward Pulse Duration 26

3.5 Circumferential Distribution - Peak Pressure 28

3.6 Circumferential Distribution - Pulse Duration 32

3.7 Engulfment Time 33

4.0 Computer Program 35

4.1 Program Logic and Structure 35

4.2 Input/Output 38

4.3 Program Listing 40

4.4 Sample Problem 40

5.0 Conclusions 61

References 63

ILLUSTRATIONS

1. Blast Wave - Vehicle Encounter Geometry 7

2. Wave Patterns with Varying Encounter Angle 9

3. Two Possible Transmitted Wave Geometries 9

4. Cone at Angle of Attack 11

5. Windward and Leeward Isobar Maps at Selected Encounter Angles. . 12

6. An Approximation to the Windward Transmitted Shock Wave. 14

7. Comparisons Between the New Model and Existing Windward Pressure Data 20

8. An Approximation to the Leeward Transmitted Shock Wave 21

9. Comparisons Between the New Model and Existing Leeward Pressure Data 23

10. Model of the Windward Pulse Duration - Regular Reflection . . . 24

11. Model of the Windward Pulse Duration - Mach Reflection 26

12. Comparisons Between the New Model and Existing Windward Pulse Duration Data 27

13. Comparisons Between the New Model and Existing Leeward Pulse Duration Data 29

14. An Approximation to the Wave Front Location 30

15. Comparisons Between the New Model and Existing Circumferential Pressure Data 31

16. Predictions of the Circumferential Distribution of Pulse Duration Made with the New Model 33

17. Total Program Flow Chart 37

1.0 INTRODUCTION

The shock-shock interaction phenomenon occurs when a supersonic vehicle encounters a shock wave. Recent interest in this problem is due to the high probability of such an occurrence during the defense of the Minuteman system by an interceptor. The threat of many reentry vehicles attacking a single target necessarily results in a fratricidal environment being created for an interceptor by the detonations of preceding interceptors. Such an encounter results in high frequency shocks transmitted through substructure which can damage components. The surface pressure is usually maximum immediately behind the wave which strikes the surface of the vehicle and then it decays to a "quasi-steady" value. The latter pressure is referred to as quasi-steady because the apparently steady conditions will actually vary as the vehicle traverses the blast sphere. However, relative to the short time it takes for the vehicle to be engulfed by the wave, the conditions behind the blast front may be assumed to be steady and the surface pressure similarly achieves a steady value. The time to decay to quasi-steady pressure is defined as the pulse duration.

The objective of this effort was to produce a relatively simple, but accurate model of the shock-on-shock phenomenon as it occurs when a sharp supersonic conical vehicle encounters a planar blast wave. The desire is to be able to predict the following features of the phenomenon, namely, the peak pressures and pulse durations produced along the windward and leeward rays of the cone and the circumferential distributions of these quantities. Any encounter angle from nose-on to broadside is permitted and the cone may be at small (less than the cone half-angle) angles of attack. The requirement for simplicity stems from the need for a low cost computer model.

The approach taken in structuring the model was to formulate a set of simplified assumptions based on the knowledge gained from: 1) the rigorous analytical results of Reference 1, 2) the test results of Reference 2, and 3) Reference 3 which presents a comparative study between these sources and established the framework for the model presented herein.

The following description of the problem (Section 2.0) is excerpted from Reference 3. Section 3.0 summarizes the current model and presents comparisons with other data sources. A listing is presented in Section 4.0 along with user information pertaining to the computerized version of the program.

2.0 THE PROBLEM - A FUNCTION OF ENCOUNTER ANGLE

The encounter between a blast wave and a supersonic vehicle produces a highly transient pressure pulse which varies in strength and duration depending on a combination of parameters: geometry and flight condition of the vehicle and the strength and orientation of the blast wave relative to the surface of the vehicle. Interest here is limited to sharp cones so the vehicle condition at a given altitude is defined by a combination of cone angle (θ_c), angle of attack (α), and vehicle velocity (V). The strength of the blast wave is defined by the ratio of the pressure behind to the pressure in front of the wave (P_2/P_1) as it travels through the atmosphere. The encounter angle (β) is defined as the angle between the blast wave and the perpendicular to the vehicle axis as shown in Figure 1.

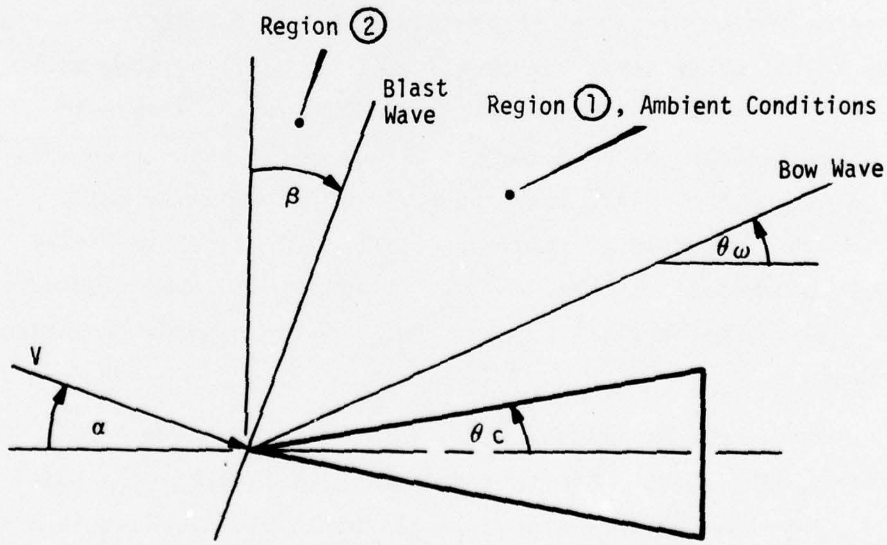

Figure 1. Blast Wave - Vehicle Encounter Geometry

The primary determinant in the level of pressure is the strength of the blast wave, but the encounter angle (β) also plays an important role. As β varies from nose-on to broadside, several distinct classes of encounters can be identified. One subdivision of encounters is marked by the bow wave angle. For β's between nose-on ($\beta=0$) and parallel to the bow wave angle (i.e., $\beta=90 - \theta_w$), the intersection of the blast and bow waves during engulfment moves from the apex of the cone aftward. For β's between ($90 - \theta_w$) and ($90 - \theta_c$), the blast-bow wave intersection moves forward along the bow wave. The two cases must be, in general, treated separately.

The range of β's between nose-on and ($90 - \theta_w$) must be subdivided further because the nature of the wave pattern which develops on the surface varies from Mach reflection to regular reflection as the encounter varies from nose-on towards broadside. The two types of wave pattern are illustrated in Figures 2a and 2b respectively. Unless a solution of the complete flow field is developed, as was done in Reference 1, the two types of wave patterns must be treated separately because there is, otherwise, no precise way of predicting the location and/or height of the Mach stem. The regular reflection pattern, on the other hand, can be solved rigorously as long as the transmitted and reflected waves are straight, i.e., immersed in uniform flow fields. As discussed in Section 3.1, the presence of gradients in the flow field leads to bending of the waves which complicates the solution of the wave pattern. It is shown that acceptable approximations are possible, however, and that good agreement is achieved between the simple model and the rigorous solution of Reference 1.

Encounters near broadside, where $(90 - \theta_w) \leq \beta \leq (90 - \theta_c)$, must also be subdivided into two subclasses depending on the orientation of the waves which emerge from the blast bow wave interaction. While the blast-bow wave intersection moves forward, the point of intercept at the vehicle surface may move from front to back depending on the orientation of the wave transmitted to the surface as shown in Figure 3.

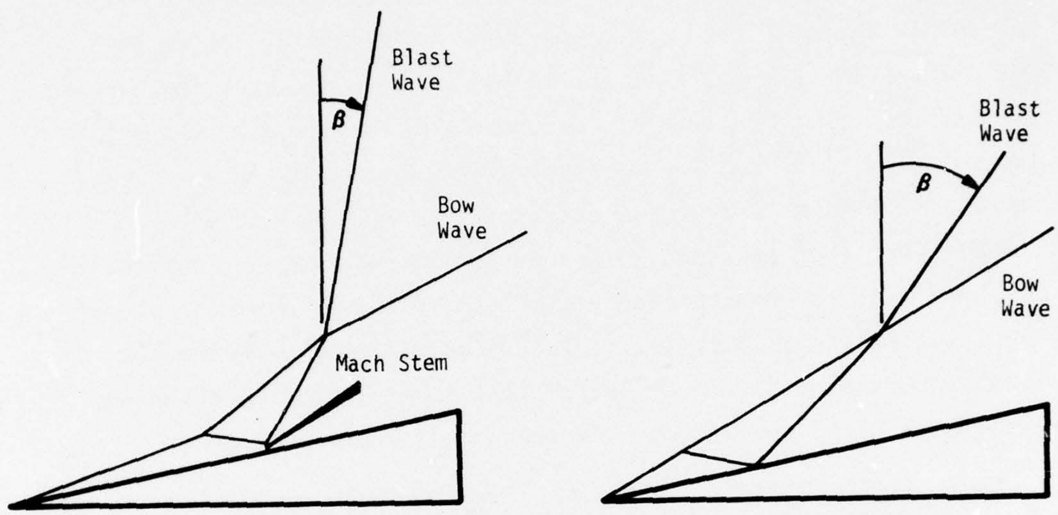

A. Mach Reflection B. Regular Reflection

Figure 2. Wave Patterns with Varying Encounter Angle

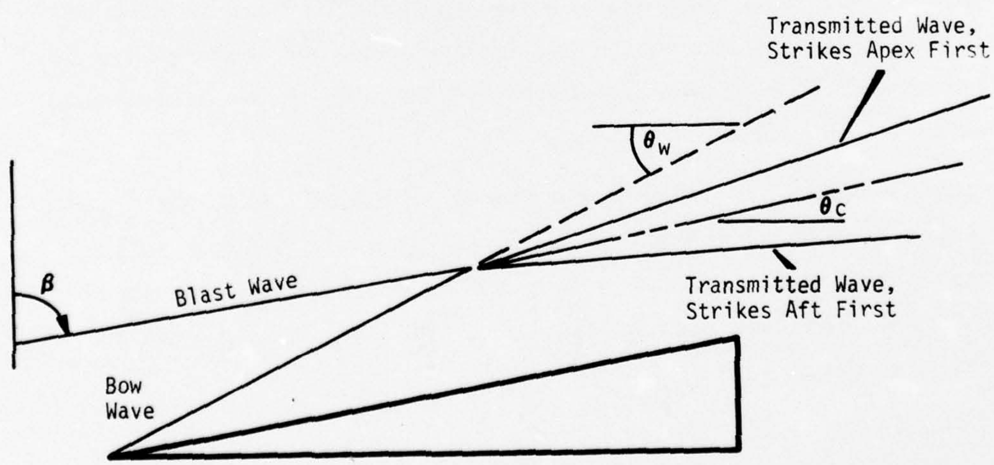

Figure 3. Two Possible Transmitted Wave Geometries

A regular reflection will occur in either case, but any attempt to model the phenomena must reflect the differences to correctly describe the velocity of the transmitted wave relative to the gas at the vehicle surface.

The complexities associated with the various subclasses of encounters are manifested in the development of models of the shock-shock phenomena. The earliest analytical success occurred for nose-on encounters which are further divided into two subclasses: sharp and blunt vehicles. The nose-on encounter of a slender sharp cone was treated by Inger in Reference 4 and the blunt body was treated successfully by McNamara and Taylor in References 5 and 6, respectively. It was possible to demonstrate the success of these solutions because of the test data available (e.g., References 7 and 8). Meanwhile, solutions were also developed for oblique encounters, but remained unverifiable until the recent sled test data became available.

Probably the highest quality experiments involving oblique encounters produced previously were the White Oak Laboratory of the Naval Surface Weapons Center using a ballistic range in combination with a shock tube. Excellent photographic data (References 9 and 10) were taken, but the use of ballistic models precluded the acquisition of actual pressure measurements. Thus, actual pressure measurements were limited essentially to nose-on encounters because of the limitations of the test techniques.

Interestingly, the sled tests cannot be used to simulate nose-on encounters because of interference between the wave and the ground. However, the sled test scheme does permit simulation of Mach stem, regular, and broadside encounters, thereby filling a large gap in the body of test data.

3.0 SHOCK-ON-SHOCK MODEL

The description of the model discussed in this section is subdivided in segments. The peak pressure on the windward ray of the cone is analyzed, followed by the model of the peak pressure on the leeward ray. The corresponding analyses of the windward and leeward pulse durations are then presented, followed by a discussion of the circumferential distributions.

The rationale presented here is used for both zero and non-zero angle of attack (α) by replacing the real cone angle (θ_c) by an effective cone (Figure 4). The windward ray analysis was performed on an effective cone with semi-vertex angle of $\theta_c+\alpha$ at zero angle of attack, while in the leeward ray analysis, the semi-vertex angle is $\theta_c-\alpha$. Similarly the bow wave angle is measured from the centerline of the effective cone.

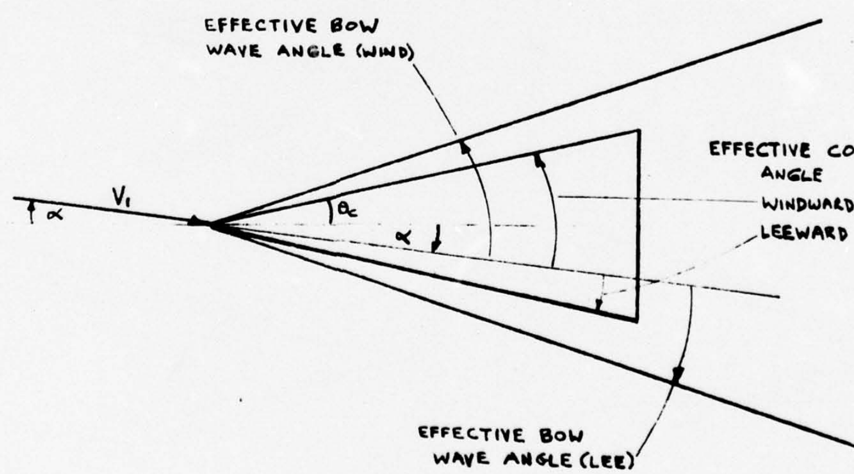

Figure 4. The Cone at Angle of Attack

3.1 Peak Windward Pressure

The starting point for the analysis was to examine some results taken from Kutler and Sakell (Reference 1) and shown in Figure 5. Figure 5 shows the isobar maps calculated with the Kutler solution for an 11.2-degree half-angle cone at Mach 5. The isobars show the shock wave patterns that result when the cone encounters a blast wave of strength 1.6 (i.e., P_2/P_1) at six different encounter angles. At the nose-on encounter (β=0), the wave transmitted to the surface is very nearly straight. As the encounter angle becomes oblique, the transmitted wave is seen to be curved. It was decided in formulating the new model referred to here that the curvature in some form should be considered.

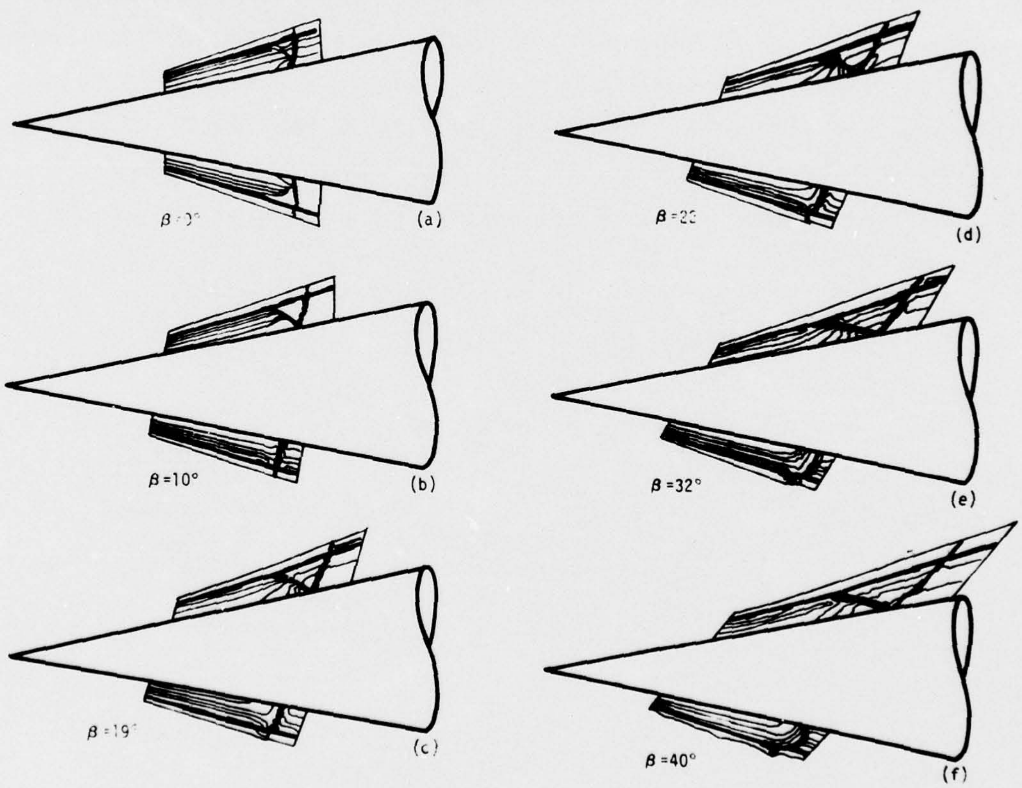

Figure 5. Windward and Leeward Isobar Maps at Selected Encounter Angles

Careful examination of the isobar maps shows that the height of the stem formed on the windward ray of the cone is relatively small in comparison to the shock layer thickness. The reflected wave bends away very quickly from being perpendicular to the surface to assume an orientation which is compatible with the new bow wave forming on the vehicle as a result of being immersed in the post-blast flow field. In fact, at all of the calculated cases except nose-on, the reflected wave bends almost immediately upon leaving the surface.

At some encounter angle between nose-on and 40 degrees, the wave pattern changes from Mach stem to regular reflection. Furthermore, as might be expected, there is no abrupt change in the wave pattern as the encounter angle changes from one which produces regular reflection to one which produces a Mach stem. Stated another way, it appears that the transmitted wave shape and orientation right down to the surface may be determined without regard for the type of reflection which will occur. If the transmitted wave is described properly, then the test for regular reflection is made at the surface and the peak pressure may be calculated accordingly, i.e., as the pressure behind a regular reflection or as the pressure behind a small normal shock located at the point of impingement of the transmitted wave on the surface.

The queston is how to solve for the bent transmitted wave in a simple fashion. The Kutler solution accomplishes this by subdividing the shock layer into many small segments and solves for the changes in flow conditions from point to point in the grid. The many points in the grid result in a more rigorous solution and increased computer cost. Noting that the transmitted wave actually is not highly curved, it was decided that the curved wave might be reasonably approximated with two straight segments as indicated in Figure 6. An iterative procedure is used to solve for the outer segment of the transmitted wave by solving the two-shock interaction at the point where the bow and blast waves intersect.

Both waves are assumed to be locally two-dimensional and their interaction results in two waves which are the beginnings of the post-encounter bow wave and the transmitted wave, respectively. The rationale used in solving the interaction of two planar waves is:

1 Assume a value for pressure jump across wave P-R (Figure 6)

2 Calculate the flow direction in region 4 (Figure 6)

3 Calculate the flow direction in region 5, assuming the pressure in region 4

4 If the flow directions in regions 4 and 5 (Figure 6) agree then the solution is found, otherwise the procedure is repeated with a new pressure jump assumed in step one.

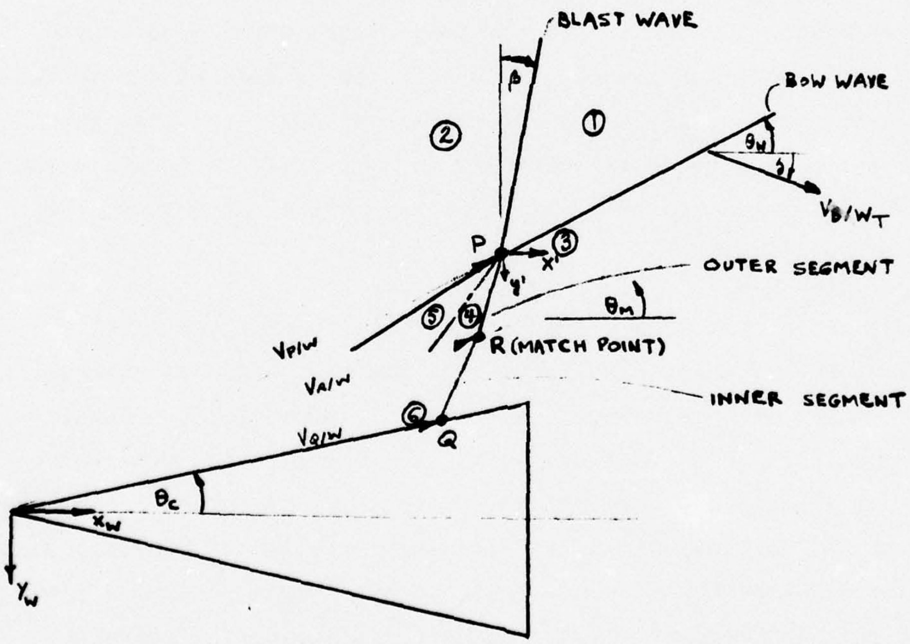

Figure 6. An Approximation to the Windward Transmitted Shock Wave

The key equations defining the above procedure are summarized below. To solve for the system of shock waves which result from the intersection of the blast and bow waves, it is useful to place the frame of reference at the point of intersection (P, Figure 6). The velocity of point P, along the bow wave, relative to the body fixed coordinates (x_W, y_W) is

$$V_{P/W} = V_{B/W_T} \frac{\cos(\beta-\delta)}{\cos(\beta+\theta_W)} \tag{1}$$

where V_{B/W_T} is the velocity of the blast relative to the body. In regions 1, 2, and 3 of Figure 6, the flow velocity components in the x' and y' directions relative to point P are

$$u_{1/P} = u_{1/W} - u_{P/W} \quad u_{2/P} = u_{2/W} - u_{P/W} \quad u_{3/P} = u_{3/W} - u_{P/W}$$

$$v_{1/P} = v_{1/W} - v_{P/W} \quad v_{2/P} = v_{2/W} - v_{P/W} \quad v_{3/P} = v_{3/W} - v_{P/W}$$

where

$$\left.\begin{array}{ll} u_{P/W} & = V_{P/W} \cos\theta_W \\ v_{P/W} & = V_{P/W} \sin\theta_W \\ u_{1/W}, v_{1/W} & = \text{Components of freestream velocity} \\ u_{2/W}, v_{2/W} & = \text{Components of post blast flow velocity} \\ u_{3/W}, v_{3/W} & = \text{Components of the shock layer velocity} \end{array}\right\} \text{relative to the body.}$$

and $\delta = \tan^{-1}\left(\frac{u_{B/W}}{v_{B/W}}\right)$.

The velocity components define the flow direction in each region. By postulating a pressure jump across the outer segment of the transmitted wave, the oblique shock relations (e.g., see Reference 11) permit calculation of the flow direction in region 4. The same shock relations are used to calculate the flow direction in region 5, on the condition that $P_5 = P_4$. This iterative procedure is continued until the flow directions in regions 4 and 5 are equal.

The outer segment of the transmitted wave, thus determined, is assumed to remain straight and of constant strength half-way into the shock layer. The match point (R, Figure 6) location and velocity ($V_{R/W}$) are determined by the point of intercept between the outer segment of the transmitted wave and the midpoint of the shock layer defined by

$$\theta_M = (\theta_W - \theta_c)/2 \tag{2}$$

and

$$V_{R/W} = V_{P/W} \frac{\sin (E_1-\theta_W)}{\sin (E_1-\theta_M)} \tag{3}$$

Knowing the pre-interaction conditions at the center of the shock layer, the pressure behind the transmitted wave outer segment is defined. The compatible inner segment is found by assigning values to the orientation of the inner segment and by calculating the resulting pressure jump at the surface. The wave strength calculated at the surface is presummed to apply along the entire inner segment and so the pressure behind the inner segment at the center of the shock layer may be calculated. The solution is found when the pressure calculated behind the inner segment at the match point agrees with the value calculated behind the outer segment. In this manner, the outer portion of the transmitted wave is consistent with the blast-bow interaction, the inner segment is consistent with the wave-surface interaction, and the two segments are compatible with each other to the extent that the pressure behind the two segments at the junction point is matched.

The calculation made at the surface begins with an attempt to find a regularly reflected wave which satisfies the condition that the flow must be parallel to the surface. If none is found, then a Mach stem, which is infinitesimal in height, is presumed to exist. That is, the stem is located at the point where the inner segment of the transmitted wave impinges on the surface. This determines the velocity of the impingement point relative to the surface ($V_{Q/W}$)

$$V_{Q/W} = V_{R/W} \frac{\sin (E_2-\theta_M)}{\sin (E_2-\theta_c)} \quad . \tag{4}$$

The velocity of the point, Q, relative to the gas on the cone surface is therefore also defined which, in turn, determines the strength of the wave travelling along the surface.

The Rankine-Hugoniot equations are then used to calculate the pressure jump across the normal shock. The key assumptions are that the transmitted wave is not so curved that a two piece representation is not adequate and that the Mach stem, when it occurs, is small in extent relative to the height of the shock layer. In principle, the matching of pressure only at the point of bending of the transmitted wave is incomplete because the flow directions should also be matched.

It was not possible to retain the simplicity of the approach and match flow directions too. Meanwhile, the comparisons with the Ames peak windward pressures at a variety of conditions show agreement to within about 10 percent. Furthermore, a considerable advantage is gained in computation time because the new model requires just a few seconds of CPU time on the IBM 370/158 at Martin Marietta's Orlando Division.

With two exceptions, the new model treats the peak windward pressure from nose-on to broadside since provision was made for the possibility for the forward moving intercept point.

One exception occurs when the blast wave is exactly parallel to the bow wave. Solving the interaction between the blast and bow waves involves defining the local flow velocities relative to the intersection of the two waves. When the waves are parallel, the intersection point velocity approaches infinity, so a solution is not possible. Loss of the solution at the single value of encounter angle is not seen to be a serious matter. The second limitation occurs at the transition encounter angle, i.e., where the wave pattern changes from Mach stem to regular reflections, because the pressure function appears to be discontinuous. Even so, the error in pressure is on the order of 10 percent. As with the Ames model, the new model has not been exercised to the point where the limits of applicability are well defined; therefore, a complete judgment of this point cannot be made at this time.

The foregoing analysis was computerized and used to calculate the peak windward ray pressures at the set of conditions which were tested during the Holloman AFB sled test program described in Reference 2 (see Table 1). For a number of the conditions, predictions are also calculated with the method of Reference 1 and provided by Kutler in Reference 12.

Table 1. Sled Test Conditions, Phases II and III

Test Number	Cone Half-Angle (Deg)	Mach Number	Angle of Attack (Deg)	Blast Strength P2/P1	Encounter Angles (Deg)
B-2*	11.2 (Model 1)	5	0	1.8	22.2, 26.3 33, 78.4
B-3				2.2	24.9, 28.8, 33.2, 78.1
B-4				2.2	24.9, 31.8, 41.2, 78.2
B-5				2.6	22.2, 28.9, 36.9, 86.5
B-6					24.7, 31.8, 45.0, 64.0
B-7	6 (Model 2)				24.8, 36.9, 44.9, 62.8
B-8	11.2 (Model 1)	2.6			24.8, 36.7, 45.0, 66.3
B-9		5	5		17.9, 21.9, 31.3, 78
B-10		5	5		28, 32, 41

*Test B-1 was aborted.

Figure 7 shows the peak windward pressures plotted against encounter angle (β) including test data, Kutler's results, and the curves produced with the model discussed here.

A number of observations are possible regarding these comparisons. Good agreement is indicated between the simple model and the rigorous solution of Kutler. There is apparently poor agreement between the calculated values and the test data. However, as explained in References 2 and 3, the test data are expected to be lower than the predictions, particularly in the Mach stem regime because the pressure data acquisition system used in the sled tests did not have a rapid enough response time to record the peak. Reference 2 shows that when the response lag is considered, the Kutler results agree very well with the test data. Therefore, the Kutler solution is treated here as the standard for comparison.

3.2 Peak Leeward Pressure

Along the leeward ray of the cone, the transmitted wave pattern is a Mach stem regardless of encounter angle. Furthermore, the Kutler results show that as the encounter angle varies from nose-on to broadside, the peak pressure does not always exceed the quasi-steady value. Thus, there is not necessarily a pressure overshoot. In this case, the pressure immediately behind the transmitted wave is less than the quasi-steady pressure and it rises monotonically to the quasi-steady value. Therefore, the approach taken in formulating the current leeward pressure model is to combine a method for calculating the pressure behind the transmitted wave with a method for calculating the quasi-steady pressure. Both quantities are calculated at each encounter angle and the applicable peak pressure is the higher of the two. Typically from $\beta=0$ (nose-on encounter) to some $\beta=\beta_{QS}$, the pressure behind the transmitted wave exceeds the quasi-steady pressure. For $\beta>\beta_{QS}$, the peak pressure is the quasi-steady value

(a)

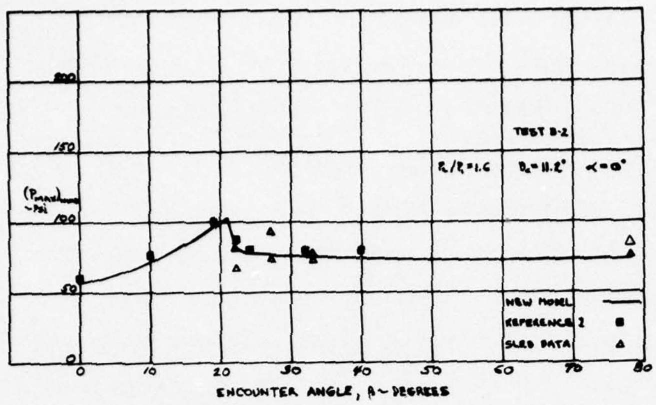

(b)

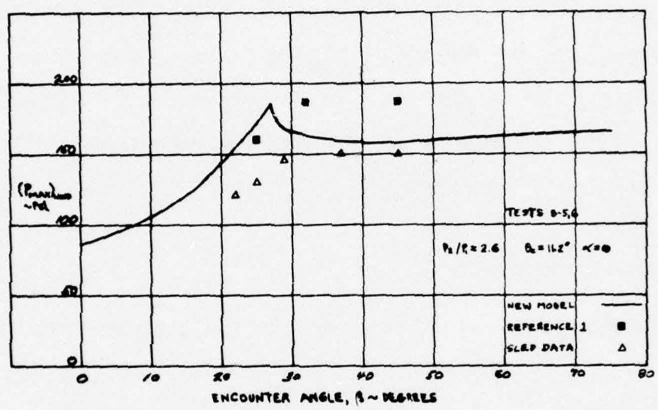

(c)

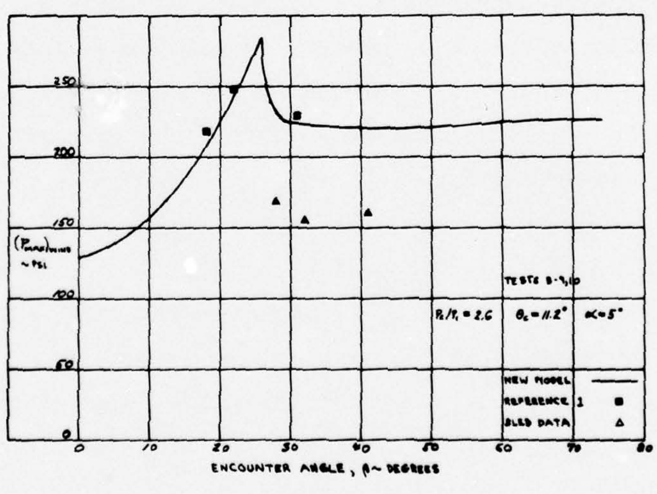

Figure 7. Comparison Between the New Model and Existing Windward Pressure Data

and, for future reference, it is noted that the pulse duration is therefore zero. As discussed earlier, the time interval in question refers to the time it takes for the pressure to decay from the peak to the quasi-steady level. Therefore, there is no shock-on-shock pulse over a portion of the leeside of the cone for a portion of the encounter angle range, and that portion is determined by comparing the pressure behind the transmitted wave to the leeward quasi-steady pressure.

The pressure behind the transmitted wave on the leeward ray is calculated with the wave pattern approximated as shown in Figure 8. This representation is simpler than that used on the windward ray and was expected to suffice because there is no transition from Mach to regular reflection and because of the knowledge gained from the windward ray analysis at $\beta=0$.

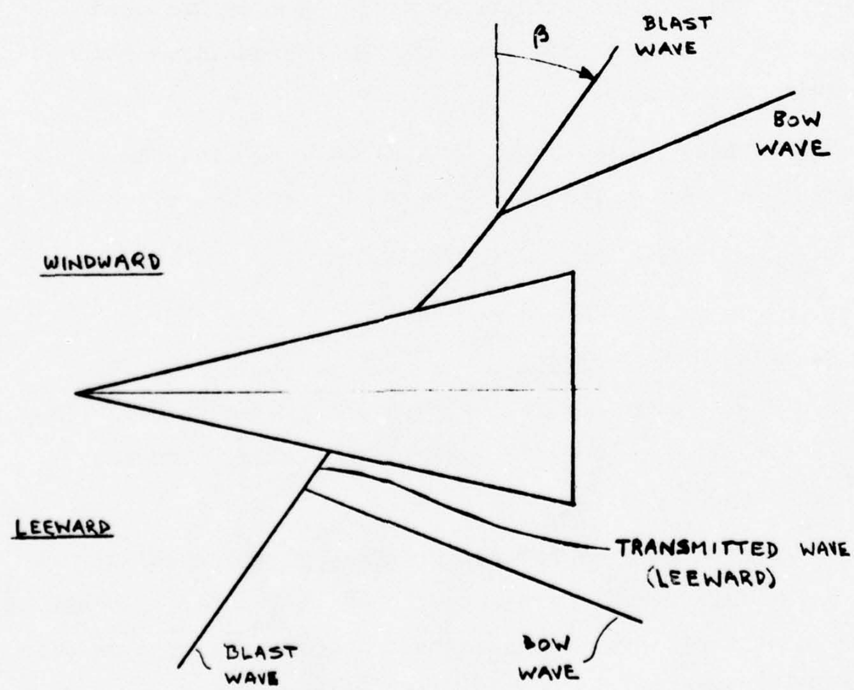

Figure 8. An Approximation to the Leeward Transmitted Shock Wave

The leeward peak pressures calculated with the simpler wave approximation are used to determine the trend with encounter angle as β increases from zero. Non-dimensionalizing the values thus obtained with the value at β=0 and then using the value calculated at β=0 with the windward analysis of Section 3.1 produces a good estimate of the leeward pressure behind the Mach stem very conveniently. The leeward analysis proceeds as follows.

The pressure behind the transmitted wave is calculated by again using the Rankine-Hugoniot relations for a normal shock. The assumption that the transmitted wave is straight defines the position and, therefore, the velocity $(V_{Q/W})_{Lee}$ of the point of impingement relative to the body surface as given by the following expression.

$$(V_{Q/W})_{Lee} = V_{B/W} \frac{\cos(\beta-\delta)}{\cos(\beta-\theta_c)} . \qquad (5)$$

The velocity of the Mach stem relative to the gas on the cone surface may then be calculated directly, thereby defining the pressure behind the stem.

The quasi-steady pressure (P_{QS}) is calculated with the following semi-empirical expression which was taken from Reference 13.

$$P_{QS} = P_2 + \frac{1}{2}\rho_2 V_2^2 \cos\gamma \left[\left(2- \frac{0.46}{M_2^2}\right)\cos\phi + \frac{0.46}{M_2^2}\right] . \qquad (6)$$

where the quantities P_2, ρ_2, V_2, M_2 are the pressure, density, velocity, and Mach number respectively of the gas behind the blast wave. The angle, γ, is the angle between the velocity vector $\overline{V}_2$ and the outward normal to the cone surface.

Figure 9 shows the peak leeward pressure plotted against encounter angle for several test cases: B-2, B-5 and 6, B-9 and 10. Comparisons with the Kutler results are included, but no test data are presented because of the poor quality of the test data in that region. Agreement between the two methods is seen to be quite good.

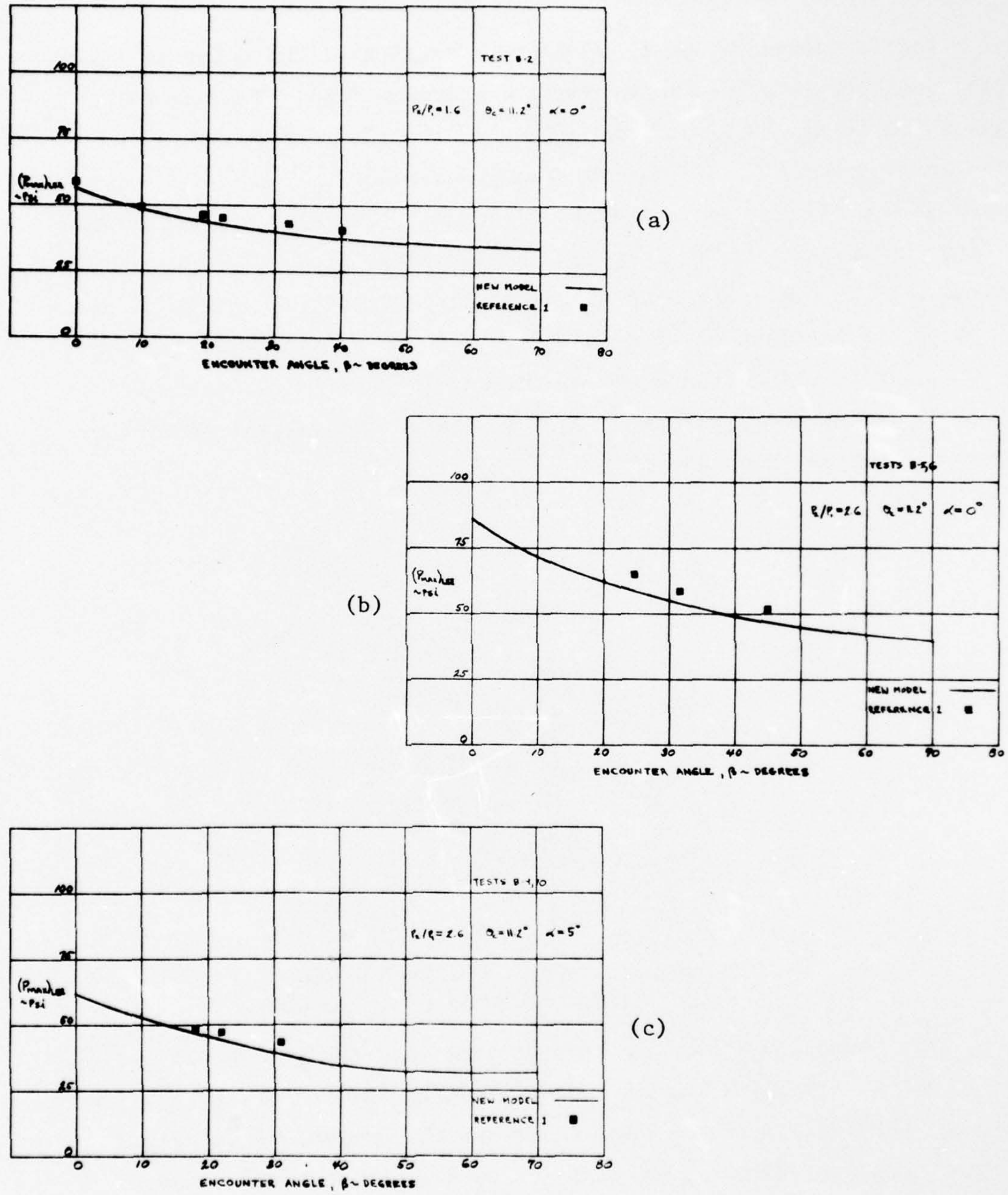

Figure 9. Comparison Between the New Model and Existing Leeward Pressure Data

3.3 Windward Pulse Duration

The formulation used to model the duration of the pulse is taken from an approach suggested by Smyrl (Reference (14). The element of gas which is at the tip of the cone when the blast arrives, is flagged and tracked as the wave propagates along the cone. The shock wave is travelling faster than the disturbed (flagged) gas and so the distance between them increases with increasing time. The flagged element of gas is the source of a secondary disturbance which is radiated at the local speed of sound (Figure 10). At any point in time, the extent to which the second disturbance has radiated, which is defined by the sonic circle, therefore bounds the region affected by the propagation shock wave.

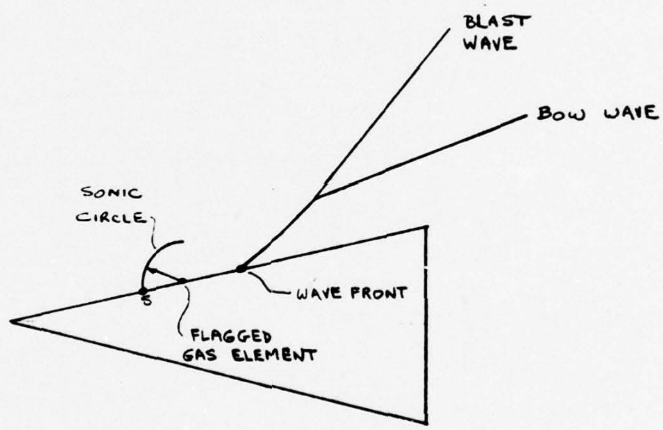

Figure 10. A Model of the Windward Pulse Duration - Regular Reflection

Smyrl suggested that the time it takes for the pressure to reach the quasi-steady level can be approximated by the difference in time between the passage of the wave front and the arrival of the sonic circle (point S, Figure 10). This reasoning was used and found to produce excessively large values in comparison to either the Kutler results or the sled test data. Therefore, the approach was modified by assuming that the secondary disturbance, namely the one emanating from the flagged gas element, is insignificant and that the quasi-steady pressure is reached when the flagged element passes the point in question. This approach gives much better agreement with the other data and therefore is implemented in the model when regular reflection occurs.

In the Mach reflection regime, this approach was found to give contradictory results in that the pulse duration appeared to decrease with increasing β. The Mach stem produces a stronger disturbance and, thus, the secondary disturbance is probably not insignificant although the duration is still overpredicted if the sonic circle reasoning is used. Therefore, a new model was formulated as follows.

The ratio of the quasi-steady pressure to the pre-encounter surface pressure defines an effective wave front which follows the actual wave front (Figure 11). The speed of the effective wave associated with the quasi-steady pressure level is defined by this pressure ratio and therefore defines an estimate of the arrival of the quasi-steady level of pressure. The pulse duration is approximated by the interval between the arrival of the actual wave front, which is known from the peak pressure analysis of Section 3.1, and the arrival of the effective wave front associated with the quasi-steady pressure.

Figure 12 presents comparisons between the current results, Kutler's calculations, and the sled test data. The figure shows the windward pulse duration plotted against encounter angles for the conditions corresponding to sled tests B-2, B-5 and 6, B-9 and 10 respectively. It should be noted that the Kutler and sled test pulse durations are taken from pressure time traces which approach the quasi-steady value asymptotically, and so the point at which the pulse ends is somewhat subjective and therefore is not always precisely defined. However, the values shown are representative and consistently arrived at and do lend credibility to this simple model.

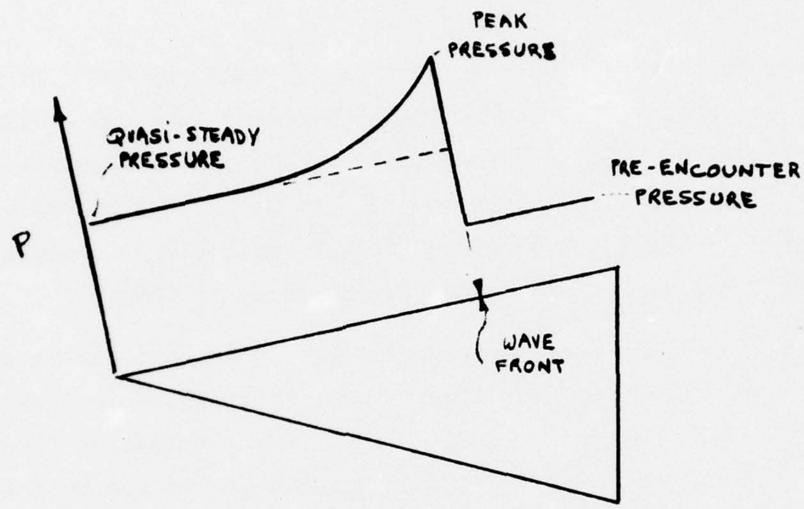

Figure 11. A Model of the Windward Pulse Duration - Mach Reflection

3.4 Leeward Pulse Duration

A very simple model was chosen for the leeward pulse duration because of the information available from the analyses previously performed. It was noted earlier that the peak leeward pressure at most encounter angles will not exceed the quasi-steady pressure and, therefore, the pulse duration is zero. The encounter angle at which the crossover occurs, labelled earlier as β_{QS}, is typically no larger than about 15 degrees. That is, the leeward pulse duration is non-zero only between $\beta=0$ (nose on) and $\beta=\beta_{QS}$. The pulse duration at $\beta=0$ is already defined by the windward analysis and so the leeward pulse duration is simply assumed to vary linearly with β from the value calculated at $\beta=0$ to zero at $\beta=\beta_{QS}$.

(a)

(b)

(c)

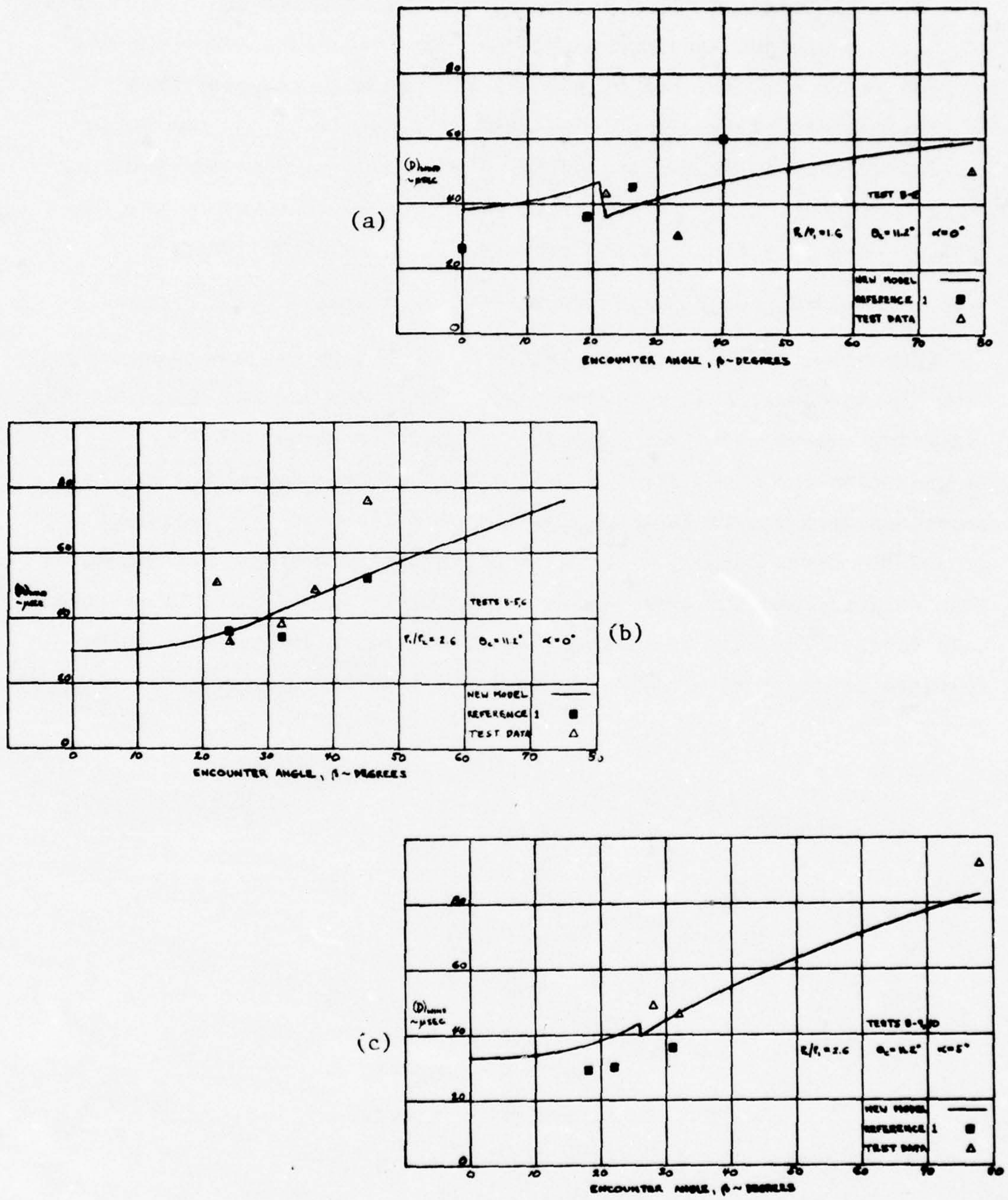

Figure 12. Comparisons Between the New Model and Existing Windward Pulse Duration Data

This approach is illustrated in Figure 13 wherein the durations are plotted against encounter angle for the conditions corresponding to sled tests B-2, B-5 and 6, B-9 and 10. As with the pressures on the leeside, there are no sled test data available and the Kutler results are all at encounter angles beyond $\beta=\beta_{QS}$, and so agreement at $\beta<\beta_{QS}$ cannot be checked. However, over most of the range of encounter angles, where the duration is zero, agreement is established.

3.5 Circumferential Distribution - Peak Pressures

The model of the circumferential distribution of peak pressure uses the information gained from the windward and leeward analyses regarding the position and velocity of the wave front. The assumption is made that the plane defined by the windward and leeward wave front locations (see Figure 14) contains the wave front at all locations around the circumference. The line of intercept between the plane, thus defined, and the cone surface is taken to be the location of the wave front. The wave front location also defines the wave velocity relative to the surface (V_Q) as given by:

$$V_Q = \frac{(1 - K_1)}{\cos\phi - K_1} (V_{Q/W})_{wind} \tag{7}$$

where

$$K_1 = \frac{1 + (V_{Q/W})_{lee}/(V_{Q/W})_{wind}}{1 - (V_{Q/W})_{lee}/(V_{Q/W})_{wind}} \tag{8}$$

$(V_{Q/W})_{wind}$, $(V_{Q/W})_{lee}$ = wave front velocities relative to the surface along the windward and leeward rays respectively.

ϕ = circumferential angle measured in a plane perpendicular to the cone axis with $\phi=0$ at the windward ray.

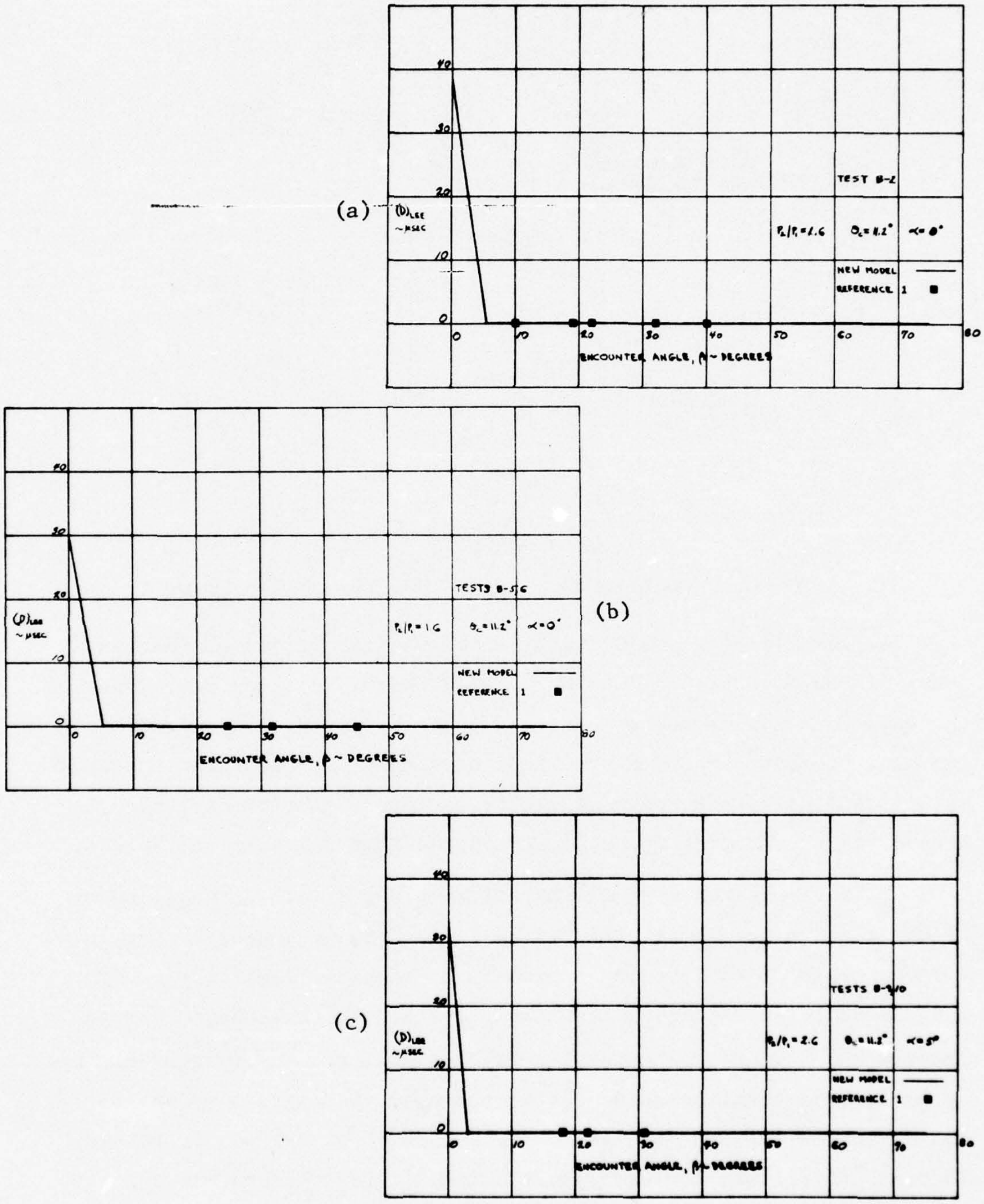

Figure 13. Comparison Between the New Model and Existing Leeward Pulse Duration Data

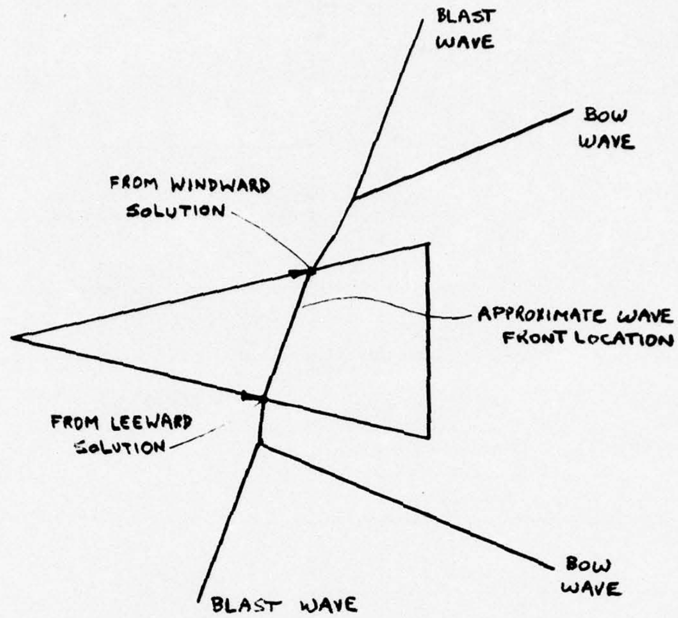

Figure 14. An Approximation to the Wave Front Location

The wave front velocity relative to the gas on the surface in front of the wave may then be calculated which, in turn, determines the wave Mach number and pressure jump by virtue of the Raskine-Hugoniot equations. Since the angle of attack is restricted to small values, the effect of angle of attack on the local flow direction is neglected in computing the velocity of the wave relative to the gas.

It is recognized that the actual wave front will actually curve around the surface so it will not be in a plane as suggested here. However, this model is seen to produce a plausible distribution of peak pressure as evidenced in Figure 15 where the calculated values are plotted against the circumferential angle, ϕ. The values obtained by Kutler and those measured during the sled tests are also shown. Again, the comparisons are presented for the B-2, B-5 and 6, B-9 and 10 test conditions, and reasonable agreement is achieved between Kutler's results and the current model.

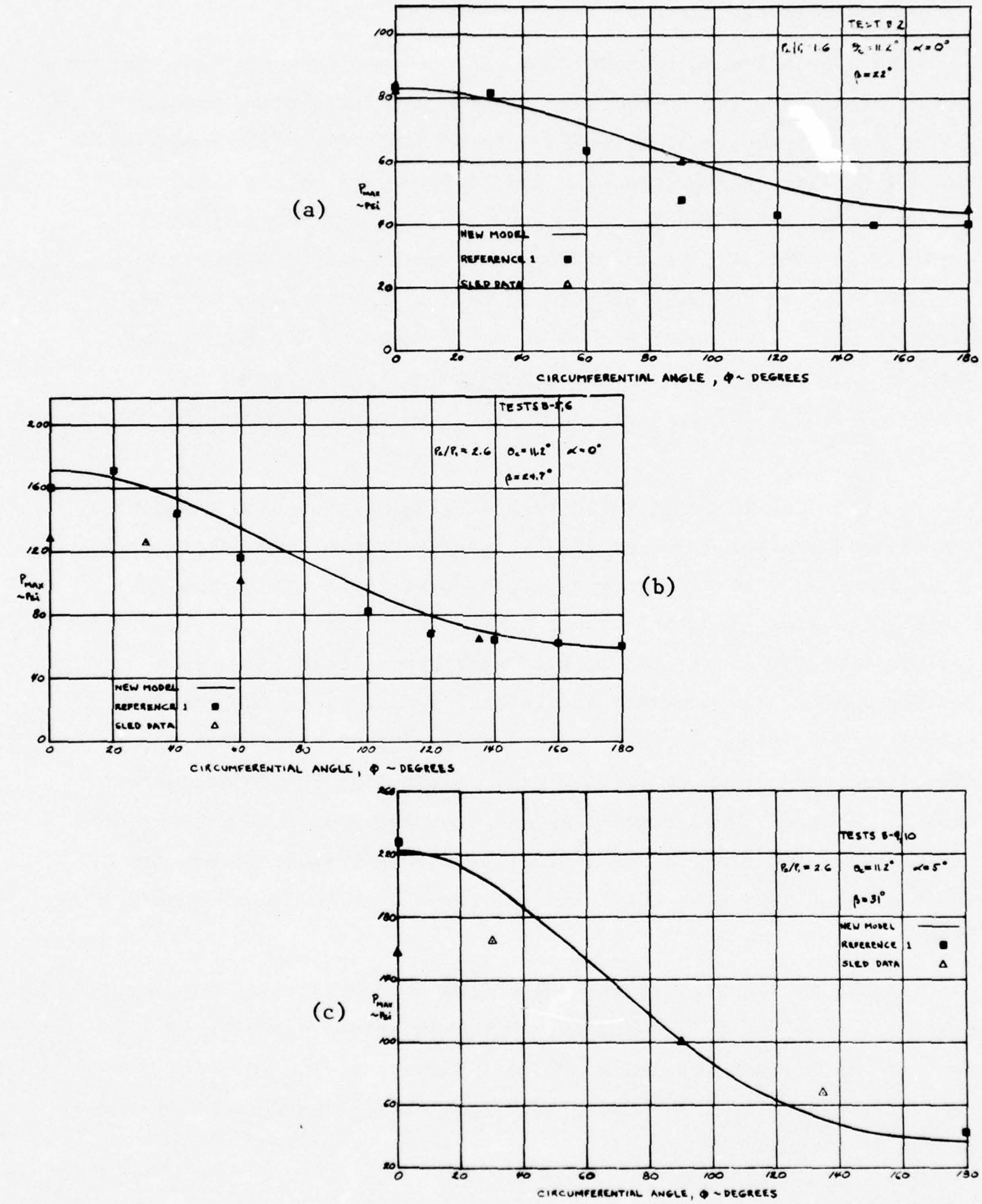

Figure 15. Comparisons Between the New Model and Existing Circumferential Pressure Data

3.6 Circumferential Distribution - Pulse Duration

The approach used to model the windward and leeward pulse durations is not easily applied to the circumferential distribution because of the difficulty in modeling the surface streamlines of the flowfield behind the blast wave. On the windward and leeward rays of the cone, the streamlines are defined because they coincide with the geometric rays of the cone. At other circumferential locations, the streamlines are curved not only because of the initial angle of attack, but also because of the angle of attack induced by the blast wave. Thus, attempting to follow a flagged element of gas cannot be achieved without solving for the entire flow field because the path is not known.

An approach is taken which is analogous to that used to model the circumferential distribution of peak pressures (see Section 3.5). It is recalled that the location of the wave front around the circumference is approximated by the surface intercept of the plane defined by the windward and leeward wave front locations. In a similar manner, the windward and leeward locations of the quasi-steady region define a plane. The surface intercept of that plane around the circumference defines an approximation to the circumferential location of quasi-steady region. The pulse duration at any circumferential location, ϕ, is defined as the time interval between the passage of the wave front and the passage of the quasi-steady "front."

Figure 16 illustrates the use of the above reasoning in sled tests B-2, B-5 and 6, B-9 and 10. Pulse durations are plotted against the circumferential angle, ϕ. Unfortunately, no other results are available for comparison from either the Kutler solution or the sled tests.

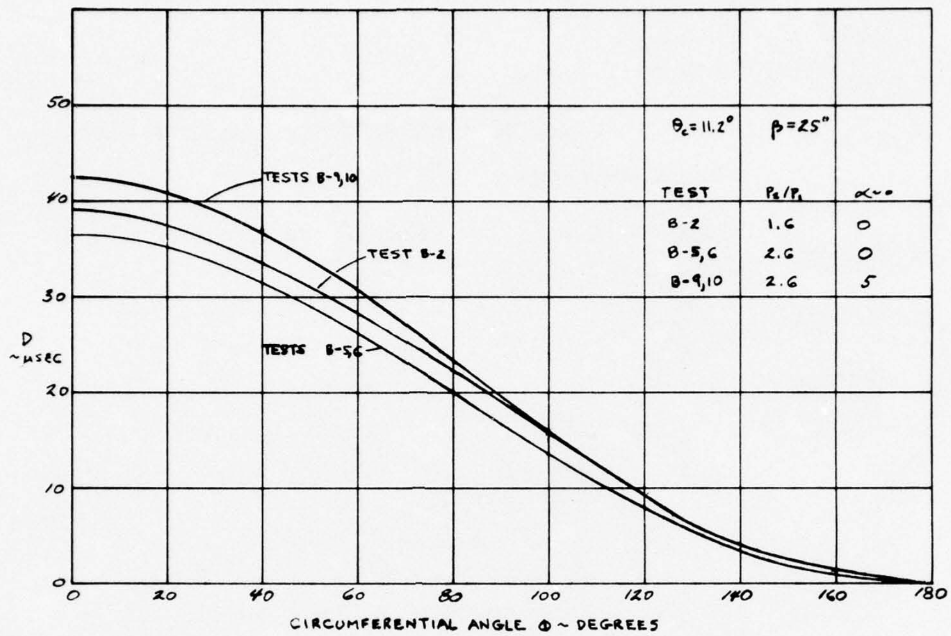

Figure 16. Typical Distributions of Pulse Duration

3.7 Engulfment Time

An additional feature of the phenomenon which is of interest to the structural dynamist is defined as the engulfment time. This quantity pertains to the passage of the wave front over a particular axial station of the body. In general, the wave front reaches the subject station first on the windward ray and last on the leeward ray. The differential time between the first and last arrival is called the engulfment time and it influences the manner in which the energy is propagated into the structure. Obviously, engulfment time is easily calculated from the results produced with the foregoing analysis because the speed of the wave front was defined at the windward and leeward rays. Therefore, the engulfment time (ENGTIM) at axial station X is given by

$$(E)_{TIM} = \frac{10^6 X}{\cos \theta_c} \left[\frac{1}{(V_{Q/W})_{lee}} - \frac{1}{(V_{Q/W})_{wind}} \right] \tag{9}$$

where

θ_c = cone half-angle

$(V_{Q/W})_{lee}$ = wave front velocity relative to the cone along the leeward ray.

$(V_{Q/W})_{wind}$ = wave front velocity relative to the cone along the windward ray.

4.0 COMPUTER PROGRAM

The analysis described in the foregoing sections was programmed on Martin Marietta's IBM 370/158 computer. The analysis was programmed using FORTRAN IV through a time sharing terminal system. The following paragraphs describe the structure, input/output features, a complete listing of the program, and a sample problem.

4.1 Program Logic and Structure

The program is designed to analyze the encounter between a supersonic sharp cone and a planar blast wave. The cone may be at a small angle of attack (α) where small is taken to mean less than the cone half-angle, and the encounter angle (β) may be anywhere from nose-on to broadside. The only encounter in this range which cannot be treated is the case where the blast wave is parallel to the bow wave. This is not a serious matter because the solution is well behaved at smaller and larger angles and is relatively insensitive to encounter angles in that regime.

The program is set up to automatically cover the entire range of encounter angles from nose-on to broadside with a predetermined increment of 5 degrees. This arrangement was chosen because the angle at which the peak pressure is highest cannot be determined a priori. Since the cost of running the program is small, the user is therefore encouraged to allow the program to find the worst condition by covering the entire range. Since there is a discontinuity in the peak pressure at the encounter angle, where transition from regular to Mach reflection occurs, the program then proceeds to perform the calculation at 1-degree intervals in the vicinity of the discontinuity to reduce the likelihood of missing the peak.

At each encounter angle, the windward peak pressure and pulse duration are calculated first followed by the analogous calculations on the leeward ray of the cone. The circumferential distributions are then evaluated and printed out.

The analysis is performed at an axial station (X) selected by the user. The station does not affect the pressure calculation because the flow field is presumed to be independent of physical scale and that the wave pattern remains self-similar as it moves down the body. The pulse duration, on the other hand, does vary with the scale of the problem because it is determined by the time required to traverse a physical distance.

Figure 17 is a flow chart for the total program. The initial decision point pertains to the encounter angle range of interest followed by a choice of branches for zero and non-zero angle of attack. Three major paths are identified by the index K. The first (K=1) treats the case of $\beta=0$ for the leeward ray of a cone at angle of attack. The cone at angle of attack is treated as an effective cone at zero α with cone angles equal to $\theta_c + \alpha$ and $\theta_c - \alpha$, respectively, at the windward and leeward rays. At $\beta=0$, using the leeward ray flow conditions and the windward ray analysis, the peak pressure and pulse duration are calculated and stored for later use in the leeward analysis at $\beta \neq 0$. If $\alpha=0$, the path K=1 is omitted.

The path K=2 treats the complete encounter angle range from nose-on to broadside. The sequence begins with the analysis of the windward ray followed by the leeward ray and finally the circumferential distribution. The sequence is initialized with the local flow conditions on the real or effective cone depending on whether or not the angle of attack is zero.

The path K=3 treats four additional encounter angles in the vicinity of the value of β at which transition from Mach to regular reflection occurs. In this way, local peak in pressure which occurs at the transition point is well defined.

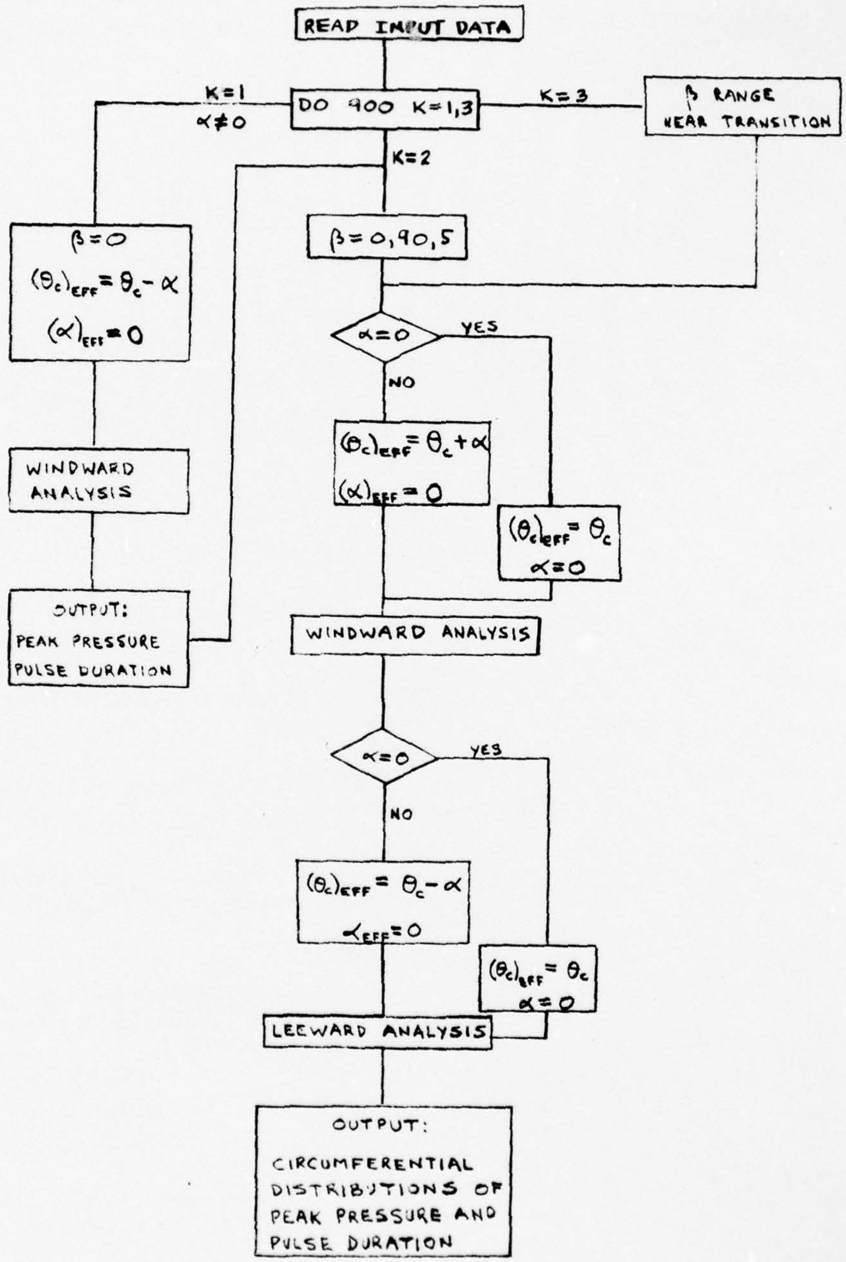

Figure 17. Total Program Flow Chart

4.2 Input/Output

Input

The following twenty quantities must be input to run the program.

Program Symbol	Definition
N	Number of blast strengths
P1	Freestream pressure, #/in^2
R1	Freestream density, #/ft^3
V1	Freestream velocity, ft/s
TC	Cone semi-vertex angle, deg
ALD	Angle of attack, deg
P2P1	Blast pressure ratio, non-dimensional
TWOD	Bow wave angle, α=0, deg
PWP10	Cone surface-to-freestream pressure ratio, $\alpha \neq 0$, non-dimensional
RWR10	Cone surface-to-freestream density ratio, α=0, non-dimensional
V3WO	Flow velocity at cone surface relative to the cone, α=0, ft/s
TWLEED	Leeward ray bow wave angle, $\alpha \neq 0$, measured from the effective cone centerline (Figure 4), deg
PWP1LE	Cone surface-to-freestream pressure ratio on the leeward ray, $\alpha \neq 0$, non-dimensional
RWR1LE	Cone surface-to-freestream density ratio on the leeward ray of the cone, $\alpha \neq 0$; non-dimensional
V3WLEE	Flow velocity on the leeward ray of cone ray surface relative to the cone, $\alpha \neq 0$, ft/s

TWWD	Windward ray bow wave angle, $\alpha \neq 0$, measured from the effective cone centerline (Figure 15), deg
PWP1W	Cone surface-to-freestream pressure ratio on the windward ray, $\alpha \neq 0$, non-dimensional
RWR1W	Cone surface-to-freestream density ratio on the leeward ray, $\alpha \neq 0$, non-dimensional
VW	Flow velocity on the windward ray of cone surface relative to the cone, ft/s
X	Axial station at which the analysis is performed, ft.

The input format for the above quantities for the usual batch processing on a computer is as follows. The sequence of inputs, as presented, must be adhered to but there is no other format restriction other than the total number of quantities on each card.

Card	Input Quantities
1	N, P1, R1, V1, TC, ALD, P2P1
2	TWOD, PWP1O, RWR1O, V3WO, TWLEED, PWP1LE, RWR1LE
3	V3WLEE, TWWD, PWP1W, RWR1W, VW, X

Output

The output information (an example of which is presented in Section 4.4) summarizes some of the input data and contains the circumferential distributions of peak pressure and pulse duration at each of the encounter angles.

The input quantities printed out are the cone semi-vertex angle, freestream velocity, angle of attack, axial station, and blast pressure ratio. At each encounter angle (β) that the analysis is performed, beginning with zero, the quantity printed first is the engulfment time (μs) followed by the distribution of pre-encounter pressure, peak shock-on-shock pressure, quasi-steady pressure, and pulse duration with circumferential body angle ϕ. It is recalled that $\phi=0$ corresponds to the windward ray. All pressures are in psi and the pulse duration is given in μs.

4.3 Program Listing

A listing of the computerized shock-on-shock model is given in the following pages. For the benefit of the user and/or programmer, a number of comments are included in the listing. The comments spell out the input quantities required to run the program, to identify major subsections of the analysis, and to define key variables.

4.4 Sample Problem

A sample problem was run to demonstrate the output format and to provide a check case. The example employs the conditions corresponding to sled tests B-9 and B-10 as listed below.

Quantity	Value	Quantity	Value
N	1	V3WO	5426.0 ft/s
P1	12.6 psi	TWLEED	13.0 deg
R1	0.0627 lb/ft^3	PWP1LE	1.69
V1	5500 ft/s	RWR1LE	1.396
TC	11.2 deg	V3WLEE	5584.0 ft/s
ALD	5.0 deg	TWWD	20.6 deg
P2P1	2.6	PWP1W	3.93
TWOD	16.6 deg	RWR1W	2.508
PWP10	2.596	VW	5375.0 ft/s
RWR10	1.95	X	1.25 ft

To reduce the volume of paper, the program was modified to produce results only at four encounter angles: 0, 20, 40, and 60 degrees. The output is presented on the facing page.

SIMPLIFIED SHOCK-ON-SHOCK MODEL

CONE HALF-ANGLE= 11.20 CONE VELOCITY= 5500.00 ANGLE OF ATTACK= 5.00
AXIAL STATION= 1.25 BLAST STRENGTH= 2.60

BETA= 0.0

ENGULFMENT TIME(MICRO-SEC)= 0.0

CIRCUMFERENTIAL ANGLE,PHI-DEG	PRE-ENCOUNTER PRESSURE-PSI	PEAK PRESSURE PSI	QUASI-STEADY PRESSURE-PSI	PULSE DURATION MICRO-SEC
0.0	49.52	128.43	117.98	33.06
20.00	48.67	126.29	115.38	32.24
40.00	46.22	120.21	108.12	29.85
60.00	42.46	111.11	97.64	26.18
80.00	37.86	100.28	85.85	21.66
100.00	32.96	89.17	74.58	16.83
120.00	28.35	79.11	65.20	12.28
140.00	24.60	71.17	58.42	8.55
160.00	22.15	66.11	54.41	6.12
180.00	21.29	64.37	53.09	5.27

BETA=20.00

ENGULFMENT TIME(MICRO-SEC)= 17.58

CIRCUMFERENTIAL ANGLE,PHI-DEG	PRE-ENCOUNTER PRESSURE-PSI	PEAK PRESSURE PSI	QUASI-STEADY PRESSURE-PSI	PULSE DURATION MICRO-SEC
0.0	49.52	223.69	145.19	38.85
20.00	48.67	215.26	140.42	37.55
40.00	46.22	192.33	127.25	33.88
60.00	42.46	160.83	108.74	28.40
80.00	37.86	127.64	88.76	21.89
100.00	32.96	98.20	70.81	15.20
120.00	28.35	75.39	57.05	9.14
140.00	24.60	59.87	48.06	4.36
160.00	22.15	51.08	43.27	1.30
180.00	21.29	48.26	41.81	0.25

BETA=40.00

ENGULFMENT TIME(MICRO-SEC)= 23.11

CIRCUMFERENTIAL ANGLE,PHI-DEG	PRE-ENCOUNTER PRESSURE-PSI	PEAK PRESSURE PSI	QUASI-STEADY PRESSURE-PSI	PULSE DURATION MICRO-SEC
0.0	49.52	219.97	169.78	52.87
20.00	48.67	210.29	162.79	51.04
40.00	46.22	184.26	143.68	45.88
60.00	42.46	149.29	117.33	38.23
80.00	37.86	113.58	89.84	29.23
100.00	32.96	83.11	66.45	20.09
120.00	28.35	60.48	49.98	11.89
140.00	24.60	45.71	40.5[illegible]	5.47
160.00	22.15	37.63	36.22	1.39
180.00	21.29	35.09	35.09	0.0

BETA=60.00

ENGULFMENT TIME(MICRO-SEC)= 25.13

CIRCUMFERENTIAL ANGLE,PHI-DEG	PRE-ENCOUNTER PRESSURE-PSI	PEAK PRESSURE PSI	QUASI-STEADY PRESSURE-PSI	PULSE DURATION MICRO-SEC
0.0	49.52	225.63	186.64	68.01
20.00	48.67	215.23	177.89	65.64
40.00	46.22	187.37	154.10	58.94
60.00	42.46	150.23	121.77	49.02
80.00	37.86	112.71	88.90	37.40
100.00	32.96	81.09	62.13	25.66
120.00	28.35	57.94	44.68	15.16
140.00	24.60	43.04	35.99	6.96
160.00	22.15	34.98	33.00	1.77
180.00	21.29	32.46	32.46	0.0

```
1
C     SIMPLIFIED SHOCK-ON-SHOCK MODEL
C
C     INPUT QUANTITIES
C
C     N=NUMBER OF BLAST STRENGTHS    P1=FREESTREAM PRESSURE,LB/IN2
C     R1=FREESTREAM DENSITY,LB/FT3   V1=FREESTREAM VELOCITY,FT/SEC
C     TC=CONE SEMI-VERTEX ANGLE,DEG.    ALD=ANGLE OF ATTACK,DEG.
C     P2P1=BLAST PRESSURE RATIO,NON DIM.
C     TWOD=BOW WAVE ANGLE,ALD=0,DEG.
C     PWP10=CONE-TO-FREESTREAM PRESSURE RATIO,ALD=0,NON DIM
C     RWR10=CONE-TO-FREESTREAM DENSITY RATIO,ALD=0,NON DIM
C     V3W0=FLOW VELOCITY AT CONE SURFACE REL. TO CONE ,ALD=0,FT/SEC
C     TWLEED=LEEWAED RAY BOW WAVE ANGLE,ALD=0,SEE FIG. 15
C     PWP1LE=CONE-TO-FREESTREAM PRESSURE RATIO,LEEWARD RAY,ALD.NE.0,NON
C     DIM
C     RWR1LE=CONE-TO-FREESTREAM DENSITY RATIO,LEEWARD RAY,ALD.NE.0,NON
C     DIM
C     V3WLEE=FLOW VELOCITY,LEEWARD RAY,REL. TO CONE,ALD.NE.0,FT/SEC
C     TWWD=WINDWARD RAY BOW WAVE ANGLE,ALD.NE.0,SEE FIG. 15,DEG.
C     PWP1W=CONE-TO-FREESTREAM PRESSURE RATIO,WINDWARD RAY,ALD.NE.0,NON
C     DIM
C     RWR1W=CONE-TO-FREESTREAM DENSITY RATIO,WINDWARD RAY,ALD.NE.0,NON
C     DIM
C     VW=FLOW VELOCITY,WIND. RAY,REL. TO CONE,ALD.NE.0,FT/SEC
C     X=AXIAL STATION AT WHICH ANALYSIS IS PERFORMED
C
C
      DIMENSION P2P2(5),P4P3(2),TBAR(2),THET4(2),THET5(2)
      P1=12.6
      R1=32.2*0.0019467
      V1=5500.
      TC=11.2
      ALD=5.
      TWOD=16.6
      PWP10=2.596
```

```
      RWRID=1.95
      V3WD=5426.
      TWLEED=13.
      PWP1LE=1.69
      RWR1LE=1.396
      V3WLEE=5584.
      TWWD=20.6
      PWP1W=3.93
      RWR1W=2.508
      VW=5375.
      X=1.25
      TCR=TC/57.3
      P2P2(1)=2.6
      P2P2(2)=1.6
      N=1
      TWLEE=TWLEED/57.3
      TWW=TWWD/57.3
C     N LOOP,NUMBER OF BLAST STRENGTHS TO BE RUN
      DO 901 NN=1,N
      P2P1=P2P2(N)
      WRITE(6,31)
   31 FORMAT(//42X,'SIMPLIFIED SHOCK-ON-SHOCK MODEL')
      WRITE(6,33)TC,V1,ALD,X,P2P1
   33 FORMAT(//5X,'CONE HALF-ANGLE=',F6.2,5X,'CONE VELOCITY=',F9.2
     *,5X,'ANGLE OF ATTACK=',F6.2,/5X,'AXIAL STATION=',F7.2,6X,'BLAST ST
     *RENGTH=',F6.2)
      IF(ALD.LE.TC) GO TO 1
      WRITE(6,2)
    2 FORMAT(2X,'*** ALPHA LARGER THAN CONE HALF-ANGLE***     ')
      GO TO 901
    1 CONTINUE
C     A1,AM1=SPD OF SND,MACH NO. IN REGION 1
      A1=SQRT(32.2*144*1.4*P1/R1)
      AM1=V1/A1
      P2P1=2.6
      AMB=SQRT((6*P2P1+1)/7)
```

```
      R2R1=(6*AMB**2)/(5.+AMB**2)
      A22=P2P1*A1**2/R2R1
      VB=AMB*A1
      KSTEM=0
      KCHECK=0
      AL=ALD/57.3
C     K SETS RANGE OF ENCOUNTER ANGLE AND ANALYSIS SEQUENCE
      DO 900 K=1,2
      IF(K.EQ.2) GO TO 26
      IF(K.EQ.3) GO TO 27
      IF(ALD.EQ.0) GO TO 900
C     K=1,BETA=0,USE WIND. RAY ANALYSIS ON LEESIDE OF CONE AT ALD
C     NOT EQUAL 0
      THETCR=TCR-ALD/57.3
      THETC=THETCR*57.3
      THETWR=TWLEE
      THETW=THETWR*57.3
      PWP1=PWP1LE
      RWR1=RWR1LE
      V3WWT=V3WLEE
      A3W2=PWP1*A1**2/RWR1
      JB1=1
      JB2=1
      JBD=0
      ALPHA=0
      ALPHAD=0
      GO TO 21
C     K=2,BETA=0,90,5---WINDWARD,LEEWARD AND CIRCUM DIST ANALYSES
C     INITIALIZE FOR WINDWARD ANALYSIS---ALD NOT ZERO
   26 THETCR=TCR+ALD/57.3
      THETWR=TWW
      THETC=THETCR*57.3
      THETW=THETWR*57.3
      PWP1=PWP1W
      RWR1=RWR1W
      V3WWT=VW
```

```
      A3W2=PWP1*A1**2/RWR1
      JB1=1
      JB2=91
      JBD=20
      ALPHAD=ALD
C     RE-INITIALIZE IF ALD EQUAL ZERO
      ALPHA=ALD/57.3
      IF(ALD.NE.0) GO TO 21
      THETCR=TCR
      THETC=TCR*57.3
      THETW=TWOD
      THETWR=TWOD/57.3
      PWP1=PWP10
      RWR1=RWR10
      V3WWT=V3W0
      A3W2=PWP1*A1**2/RWR1
      GO TO 21
C     K=3,SET BETA RANGE NEAR TRANSITION,REPEAT COMPLETE ANALYSIS
   27 JB1=BSTEM+2
      JB2=BSTEM+5
      JBD=1
      KSTEM=0
   21 CONTINUE
      PMP1=.95*PWP1
      THETA=(THETW+THETC)/2
      AM1ST=V1*SIN(THETWR)/A1
      P3P1=(7*(AM1ST**2)-1)/6
      U3WW=V3WWT*COS(THETCR)
      V3WW=-V3WWT*SIN(THETCR)
C     ENCOUNTER ANGLE(BETA) LOOP
      DO 802 JB=JB1,JB2,JBD
      BETAD=JB-1
      BETA=BETAD/57.3
      BE=BETA-ALPHA
      BED=BE*57.3
      BCR=19.
```

```
      IF((90-BED).LE.THETC) GO TO 802
      IF(K.EQ.1)GO TO 42
   23 WRITE(6,17)BETAD
   17 FORMAT(/42X,'BETA=',F5.2)
   42 CONTINUE
      BBOWD=90.-THETW
      BBOW=BBOWD/57.3
      IF(BED.NE.BBOWD) GO TO 12
      WRITE(6,11)
   11 FORMAT(2X,'NO SOLUTION-BLAST PARALLELS BOW WAVE')
      GO TO 802
   12 CONTINUE
      ANGLE=90-(BE+THETWR)*57.3
      AMBSB=AMB*SIN(BE)
      UBW=VB*COS(BE)+V1
C     VELOCITIES(V) AND FLOW DIRECTIONS(THET) ARE LABELLED BY FLOW
C     FIELD REGION,E.G.,V2W=Y COMP. OF VEL. IN REGION 2 REL TO CONE(W)
C     V2WT=TOTAL VEL IN REGION 2,REL TO CONE
C     THET4=FLOW DIRECTION IN REGION 4 REL. TO BODY FIXED X AXIS
      VBW=VB*SIN(BE)
      VBWT=(UBW*UBW+VBW*VBW)**.5
      DEL=ATAN(VBW/UBW)
      BMD=BE-DEL
      DMB=DEL-BE
      BPTW=BE+THETWR
      VPWT=VBWT*COS(BMD)/COS(BPTW)
      IF(BE.LT.BBOW) GO TO 14
      VPWT=-VBWT*COS(DMB)/COS(BPTW)
      UPW=-VPWT*COS(THETWR)
      VPW=VPWT*SIN(THETWR)
      GO TO 13
   14 UPW=VPWT*COS(THETWR)
      VPW=-VPWT*SIN(THETWR)
   13 V2BT=VB-(144*32.2*P1*(P2P1-1.)/(R1*VB))
      U2W=(VB-V2BT)*COS(BE)+V1
      V2W=(VB-V2BT)*SIN(BE)
```

```
      VN1W=V1*SIN(THETWR)
      VT3W=V1*COS(THETWR)
      VN3W=VN1W-(((P3P1-1)*12.5*144*32.2)/(R1*VN1W))
      GA=ATAN(VN3W/VT3W)
      V3WT=V1*COS(THETWR)/COS(GA)
      U3W=V3WT*COS(THETWR-GA)
      V3W=-V3WT*SIN(THETWR-GA)
C     VELOCITIES REL TO P(INTERSECTION BETWEEN BOW AND BLAST WAVE)
      U1P=V1-UPW
      V1P=-VPW
      V1PT2=U1P*U1P+V1P*V1P
      AM1P2=V1PT2/(A1*A1)
      U2P=U2W-UPW
      V2P=V2W-VPW
      V2PT2=U2P*U2P+V2P*V2P
      U3P=U3W-UPW
      V3P=V3W-VPW
      V3PT2=U3P*U3P+V3P*V3P
C     FLOW DIRECTIONS
      THET1=ABS(ATAN(V1P/U1P))
      IF(BE.LT.BBOW) GO TO 62
      AL13=THETWR-THET1
      GO TO 63
C     ANGLE AL13 REFERS TO THE WAVE SEARATING REGIONS 1 AND 3
C     MEASURED BETWEEN FLOW IN REGION 1(THET1) AND THE WAVE
   62 AL13=THET1-THETWR
   63 AM1S32=AM1P2*SIN(AL13)*SIN(AL13)
      CDEL13=(((1.2*AM1P2)/(AM1S32-1))-1)*TAN(AL13)
      XCD13=1./CDEL13
      DEL13=ATAN(XCD13)
C     ANGLE DEL13 REFERS TO THE CHANGE IN FLOW DIRECTION IN GOING
C     FROM REGION 1 TO REGION 3
      IF(BE.LT.BBOW) GO TO 64
      THET3=THET1+DEL13
      AL12=THET1-90./57.3+BE
      GO TO 65
```

```
   64 THET3=THET1-DEL13
      AL12=90./57.3-(THET1+BE)
   65 AM1SA2=AM1P2*SIN(AL12)*SIN(AL12)
      CDEL12=(((1.2*AM1P2)/(AM1SA2-1))-1)*TAN(AL12)
      XCD12=1./CDEL12
      DEL12=ATAN(XCD12)
      IF(BE.LT.BBOW) GO TO 66
      THET2=THET1-DEL12
      GO TO 67
   66 THET2=THET1+DEL12
   67 A3A12=(7.*AM1P2*(SIN(AL13))**2.-1.)*(AM1P2*(SIN(AL13))**2.+5.)
     */(36.*AM1P2*(SIN(AL13))**2.)
      A32=A3A12*A1*A1
      AM3P2=V3PT2/A32
      AM2P2=V2PT2/A22
      PUP1=(7.*AM3P2-1.)/6.
      PUP2=P2P1*(7.*AM2P2-1.)/(P3P1*6.)
      IF(PUP2.GT.PUP1) GO TO 51
   50 P4P3UP=PUP2
      GO TO 52
   51 P4P3UP=PUP1
   52 P4P3(2)=P2P1*.95
C     CHOOSE(ITERATE) P4P3 SO AS NOT TO EXCEED THEO.LIMITS PUP1
C     OR PUP2
      IF(P2P1.LE.P4P3UP)GO TO 59
      P4P3(2)=P4P3UP*.95
   59 JMAX=P2P1*100000
      DO 53 J=1,JMAX
      AL34=ASIN(SQRT((6.*P4P3(2)+1.)/(7.*AM3P2)))
  998 AM3SA2=AM3P2*SIN(AL34)*SIN(AL34)
      CDEL34=(((1.2*AM3P2)/(AM3SA2-1))-1)*TAN(AL34)
      XCD34=1./CDEL34
      DEL34=ATAN(XCD34)
      IF(BE.LT.BBOW) GO TO 68
      THET4(2)=THET3-DEL34
      GO TO 69
```

```
68 THET4(2)=THET3+DEL34
69 V4V32=1.-(5./36.)*(AM3SA2-1.)*(7.*AM3SA2+5.)/(AM3P2*AM3SA2)
   V4PT2=V4V32*V3PT2
   P3P2=P3P1/P2P1
   P5P2=P4P3(2)*P3P2
   AL52=ASIN((6.*P5P2+1.)/(7.*AM2P2))**.5
   AM2SA2=AM2P2*SIN(AL52)*SIN(AL52)
   CDEL52=(((1.2*AM2P2)/(AM2SA2-1))-1)*TAN(AL52)
   XCD52=1./CDEL52
   DEL52=ATAN(XCD52)
   IF(BE.LT.BBOW) GO TO 80
   THET5(2)=THET2+DEL52
   GO TO 81
80 THET5(2)=THET2-DEL52
81 V5V22=1.-5./36.*(AM2SA2-1.)*(7.*AM2SA2+5.)/(AM2P2*AM2SA2)
   V5PT2=V5V22*V2PT2
C  EXAMINE DIFFERENCE IN FLOW DIRECTIONS(TBAR) BET. REGIONS
C  4 AND 5. IF ACCEPTABLE GO TO 4.
C  ADJUSTMENTS TO P4P3 DEPENDS ON SIGN AND SLOPE OF TBAR
   TBAR(2)=THET5(2)-THET4(2)
   IF(ABS(TBAR(2)).LE.0.00005) GO TO 4
   IF(J.GT.1) GO TO 54
   P4P3(1)=P4P3(2)
   P4P3(2)=P4P3(2)-0.02
   TBAR(1)=TBAR(2)
   GO TO 53
54 DTDP=(TBAR(2)-TBAR(1))/(P4P3(2)-P4P3(1))
   IF(J.GT.2) GO TO 82
   B=TBAR(2)-P4P3(2)*DTDP
   P4P3(2)=-B/DTDP
   IF(P4P3(2).LE.1.0) GO TO 57
   GO TO 53
82 IF(BE.GT.45./57.3) GO TO 57
   IF(ABS(DTDP).LE.0.0001) GO TO 4
57 IF(TBAR(2).GT.0.0.AND.DTDP.GT.0.0) GO TO 55
   IF(TBAR(2).GT.0.0.AND.DTDP.LT.0.0) GO TO 56
```

```
      IF(TBAR(2).LT.0.0.AND.DTDP.GT.0.0) GO TO 56
      IF(TBAR(2).LT.0.0.AND.DTDP.LT.0.0) GO TO 55
   55 P4P3(1)=P4P3(2)
      P4P3(2)=P4P3(2)-0.00001
      TBAR(1)=TBAR(2)
      GO TO 53
   56 P4P3(1)=P4P3(2)
      P4P3(2)=P4P3(2)+0.00001
      TBAR(1)=TBAR(2)
      GO TO 53
   53 CONTINUE
      GO TO 900
    4 CONTINUE
C     BLAST-BOW WAVE INTERSECTION SOLVED
      IF(BE.LT.BBOW) GO TO 70
      EIR=THET3-AL34
      EI=EIR*57.3
      GO TO 71
   70 EIR=THET3+AL34
      EI=EIR*57.3
   71 CONTINUE
C     IF BETA IS BETWEEN (90-THETW) AND (90-THETC),ASSUME TRANS.
C     WAVE IS UNAFFECTED BY SHOCK LAYER AND OMIT INNER SEG. SOL.
C     SOLUTION OF INNER SEG. OF THE TRANS. WAVE IS BEGUN AT 105
      IF(BE.LT.BBOW) GO TO 105
      IF(EI.LT.THETC) GO TO 105
      AMT32=(6.*P4P3(2)+1.)/7.
      VT3T=SQRT(AMT32)*SQRT(A3W2)
      UT3=VT3T*SIN(EIR)
      VT3=VT3T*COS(EIR)
      UTW=UT3+U3WW
      VTW=VT3+V3WW
      VTWT2=(UTW*UTW+VTW*VTW)
      VTWT=SQRT(VTWT2)
      Y=ATAN(VTW/UTW)
      VONT2=VTWT*SIN(EIR+Y)/SIN(EIR-THETCR)
```

```
      UOW=VOWT2*COS(THETCR)
      VOW=-VOWT2*SIN(THETCR)
      U3O=U3WW-UOW
      V3O=V3WW-VOW
      AM3O2=(U3O*U3O+V3O*V3O)/A3W2
      P4P3IN=P4P3(2)
      AL34W=E1R-THETCR
      SAL34W=SIN(AL34W)*SIN(AL34W)
      GO TO 101
C *****DEFINE CONDITIONS IN INNER LAYER
C     P4OUT=PRESSURE AT MATCH POINT(R) BEHIND THE OUTER SEGMENT
C     OF THE TRANS. WAVE,P4IN=CORRESP. PRESSURE FOR INNER SEGMENT
  105 P4OUT=P4P3(2)*PMP1*P1
      THETO=THETM
      IF(BED.GT.BCR) GO TO 83
      THETO=.99*THETW+BETAD*(THETM-.99*THETW)/BCR
   83 THETOR=THETO/57.3
      IF(BE.LT.BBOW )GO TO 72
      E2=-90.
      GO TO 73
   72 E2=THETO
   73 L=0
      DO 700 N=1,180
      E2=E2+1.
   84 E2R=E2/57.3
      E1MTW=E1R-THETWR
      E1MTO=E1R-THETOR
      VRWT=VPWT*SIN(E1MTW)/SIN(E1MTO)
      E2MTO=E2R-THETOR
      E2MTC=E2R-THETCR
      VOWT2=VRWT*SIN(E2MTO)/SIN(E2MTC)
      IF(BE.LT.BBOW) GO TO 75
  100 UOW2=-VOWT2*COS(THETCR)
      VOW2=VOWT2*SIN(THETCR)
      GO TO 76
   75 UOW2=VOWT2*COS(THETCR)
```

```
      VOW2=-VOWT2*SIN(THETCR)
   76 U3Q=U3W-UOW2
      V3Q=V3W-VOW2
      AM3Q2=(U3Q*U3Q+V3Q*V3Q)/A3W2
      AM3Q=SQRT(AM3Q2)
C     CALCULATE INNER SEGMENT PRESSURE
   77 AL34W=E2R-THETCR
   78 SAL34W=SIN(AL34W)*SIN(AL34W)
      P4P3IN=(7.*AM3Q2*SAL34W-1.)/6.
      P4IN=P4P3IN*PMP1*P1
C     EXAMINE DIFFERENCE(DP) BETWEEN P4OUT AND P4IN, WHEN ACCEPT.
C     THEN INNER SEGMENT IS DEFINED
      DP=P4IN-P4OUT
      IF(ABS(DP).LE.0.01) GO TO 701
      IF(BE.LT.BBOW) GO TO 74
      IF(DP.GT.0.0) GO TO 700
      E2=E2-0.0001
      L=L+1
      IF(L.GE.10000) GO TO 701
      GO TO 84
   74 IF(DP.LT.0.0) GO TO 700
      E2=E2-0.0001
      L=L+1
      IF(L.GE.10000) GO TO 701
      GO TO 84
  700 CONTINUE
  701 CONTINUE
C     INNER SEGMENT OF TRANS. WAVE DEFINED,NOW DETERMINE IF
C     REGULAR REFLECTION AT SURFACE IS POSSIBLE BY FINDING
C     REFLECTED WAVE ANGLE AL46
  101 AM4Q2=(AM3Q2*(6.*P4P3IN+1.)-5.*(P4P3IN**2-1.))/(P4P3IN*(P4P3IN+6
     *.))
      IF(AM4Q2.GT.1.) GO TO 702
      GO TO 122
  702 AM4Q=SQRT(AM4Q2)
      SAMD2=(P4P3IN+6.)/(7.*P4P3IN*AM4Q2)
```

```
      AMD34=ASIN(SQRT(SAMD2))
      DEL34M=AL34M-AMD34
      DEL46R=DEL34M
      M=0
      AL46=0.2/57.3
      REG=0
      DO 120 JJ=1,90
      AL46=AL46+1./57.3
  704 AM4SA2=AM402*(SIN(AL46))*SIN(AL46)
      CDEL46=(((1.2*AM402)/(AM4SA2-1))-1)*TAN(AL46)
      XCD46=1./CDEL46
      DEL46=ATAN(XCD46)
      IF(DEL46.LE.0.0) GO TO 120
      ALMDEL=AL46-DEL46
      AM62=(1./((SIN(ALMDEL))*SIN(ALMDEL)))*(AM4SA2+5.)/(7.*AM4SA2-1)
      IF(AM62.LE.1.0) GO TO 120
      DCRIT=0.0001
      DDEL46=DEL46-DEL46R
      IF(ABS(DDEL46).LE.DCRIT) GO TO 130
      IF(DDEL46.LT.0.0) GO TO 120
      AL46=AL46-0.001/57.3
      M=M+1
      IF(M.GT.10000) GO TO 122
      GO TO 704
  120 CONTINUE
C     IF REG REFLECTION NOT POSSIBLE, GO TO MACH STEM SOLUTION
C     OTHERWISE CALCULATE REG. REF. PRESSURE P6
      GO TO 122
  130 BCR=19
      REG=1
      SAL462=(SIN(AL46))*SIN(AL46)
      P6P4=(7*AM402*SAL462-1)/6
      P6=P6P4*P4P3(2)*PWP1*P1
      PMAXP1=P6/P1
C     REGULAR REFLECTION DURATION(DREG)
      AL46=AL46*57.3
```

```
      DEL46=DEL46*57.3
      R4R3=(6.*AM3Q2*SAL34W)/(AM3Q2*SAL34W+5.)
      R6R4=(6.*AM4SA2)/(AM4SA2+5.)
      R6R3=R6R4*R4R3
      P6P3=P6P4*P4P3(2)
      A62=A3W2*P6P3/R6R3
      V60=-SQRT(AM62)*SQRT(A62)
      V6W=V60+ABS(VQWT2)
      AMQEFF=SQRT((6.*P6P3+1.)/7.)
      VQ3EFF=AMQEFF*SQRT(A3W2)
      VQWEFF=VQ3EFF+V3WWT
   91 DREG=(1000000.*X/COS(THETCR))*(1./V6W-1./VQWEFF)
C     SKIP OVER MACH SOLUTION SINCE REG. REF. OCCURRED
      GO TO 800
C     MACH STEM PRESSURE(PNS) AND PULSE DURATION(DNS)
  122 BSTEM=BETAD
      B=1.
      IF(AL.NE.O.AND.K.NE.1) B=1.1
      P4P3NS=(7.*AM3Q2-1.)/6.
      P4P3NS=P4P3NS*B
      AM3Q2=(6.*P4P3NS+1.)/7.
      R6R3=6.*AM3Q2/(AM3Q2+5.)
      A62=A3W2*P4P3NS/R6R3
      AM6Q2=(AM3Q2+5.)/(7.*AM3Q2-1.)
      V6Q=-SQRT(AM6Q2)*SQRT(A62)
      V6W=V6Q+ABS(VQWT2)
      VBW=-SQRT(A62)+V6Q+VQWT2
      VQ3EFF=SQRT(AM3Q2)*SQRT(A3W2)
      VQWEFF=VQ3EFF+V3WWT
C     STEM VELOCITY REL. TO CONE FLOW(VQ3EFF AND REL . TO CONE
C     SURFACE(VQWEFF)
      U2W=(VB-V2BT)*COS(BETA)+V1*COS(AL)
      V2W=(VB-V2BT)*SIN(BETA)+V1*SIN(AL)
C     DEFINE QUASI STEADY CONDITIONS BEHIND MACH STEM
      ALE=ATAN(V2W/U2W)
      V2WT=(U2W*U2W+V2W*V2W)**.5
```

```
      AM2=V2WT/SQRT(A22)
      BK=COS(ALE)*SIN(TCR)
      CK=SIN(ALE)*COS(TCR)
      CGAM=BK+CK
      PA=P2P1*P1
      POS=PA+.5*R2R1*R1*V2WT**2*CGAM*((2-.46/AM2)*CGAM+.46/AM2)/(
     *144*32.2)
      POSPW=POS/(PWP1*P1)
      AMOS=(6*POSPW+1.)/7.
      V3OS=SQRT(AMOS)*SQRT(A3W2)
      ROSRW=6*AMOS/(AMOS+5.)
      VOSO=V3OS+V3WT
      AOS2=A3W2*POSPW/ROSRW
      AMOS6=(AMOS+5.)/(7*AMOS-1.)
      VOS6=-SQRT(AMOS6)*SQRT(AOS2)
      VOS6W=VOS6+VOSO
C     QUASI STEADY PRESSURE(POS),VELOCITY REL. TO CONE(VOS6W)
      T=1000000*X/(COS(TCR)*VOWEFF)
      DNS=(VOWEFF-VOS6W)*T/VOS6W
      PMAXNS=P4P3NS*PWP1*P1
      PMAXP1=PMAXNS/P1
      IF(ALPHA.EQ.0..AND.BETA.EQ.0) GO TO 5
C     PLEEO,DLEEO ARE PRESSURE AND DURATION AT BETA=0 CALCULATED WITH
C     WINDWARD ANALYSIS,USED TO SCALE MORE APPROX LEE PRESSURES
      GO TO 800
    5 PLEEO=PMAXNS
      DLEEO=DNS
      IF(K.EQ.1) GO TO 900
  800 CONTINUE
C     INITIALIZE FOR LEEWARD ANALYSIS
      IF(ALD.EQ.0) GO TO 38
      PWP1L=PWP1LE
      RWR1L=RWR1LE
      V3WL=V3WLEE
      GO TO 37
   38 CONTINUE
```

```
      PWP1L=PWP10
      RWR1L=RWR10
      V3WL=V3W0
C     DEFINE BETA=BOS WHERE PRESSURE BEHIND STEM(PSTEM)=QUASI
C     STEADY PRESSURE(POS)
   37 AW2L=PWP1L*A1**2/RWR1L
      IF(KCHECK.EQ.1) GO TO 25
      A=1.
C     DEFINE XBETA AND OTHER X SUBSCRIPTED VARIABLES AS DUMMIES
C     FOR THE CALCULATION OF BOS
      DO 24 MP=1,90
      XBETA=(MP-1)/57.3
      XBETAD=XBETA*57.3
      XBE=XBETA-ALD/57.3
      U=VB*COS(XBE)+V1
      V=VB*SIN(XBE)
      VBWTX=(U*U+V*V)**.5
      D=ATAN(V/U)
      BMD=XBE-D
      BMT=XBETA-TCR
      VQWX=VBWTX*COS(BMD)/COS(BMT)
      VQ3X=VQWX-V3WL
      AMQX2=VQ3X*VQ3X/AW2L
      P6P3X=(7*AMQX2-1)/6.
      PSTEM=P6P3X*PWP1L*P1
      IF(XBETA.NE.0) GO TO 7
C     PREF IS LEESIDE PRESSURE(PLEE) AT BETA=0 CALCULATED WITH
C     TRANS. WAVE ASSUMED STRAIGHT,USED TO NON DIM. LEESIDE PRESS.
      PREF=PSTEM
    7 CONTINUE
      PSTEM=PSTEM*PLEEO/PREF
      U2WX=(VB-V2BT)*COS(XBETA)+V1*COS(AL)
      V2WX=(VB-V2BT)*SIN(XBETA)+V1*SIN(AL)
      ALE=ATAN(V2WX/U2WX)
      THETE=TCR-AL
      V2WTX=(V2WX*V2WX+U2WX*U2WX)**.5
```

```
      AM2=V2WTX/SQRT(A22)
      CPHI=SIN(TCR)*COS(ALE)-COS(TCR)*SIN(ALE)
      PA=P2P1*P1*A
      PB=.5*R2R1*R1*V2WTX**2.*CPHI*((2.-.46/AM2)*CPHI+.46/AM2)/(144*32.2
     *)
      POS=PA+PB
      IF(PSTEM.LT.POS) GO TO 23
      IF(MP.GT.21) GO TO 23
   24 CONTINUE
C     BETA AT WHICH PRESS. BEHIND STEM EQUALS QUASI STEADY PRESS.
C     (BOS) IS DEFINED HERE
   23 BOS=XBETA
      KCHECK=1
      IF(BOS.LT.0.087) BOS=0.087
      BOSD=BOS*57.3
C     CALCULATE LEEWARD PRESSURE(PLEE) AND DURATION(DURALE)
   25 CONTINUE
      U=VB*COS(BE)+V1
      V=VB*SIN(BE)
      VBWT=(U*U+V*V)**.5
      D=ATAN(V/U)
      BMD=BE-D
      BMT=BETA-TCR
      VOWLEE=VBWT*COS(BMD)/COS(BMT)
      VO3LEE=VOWLEE-V3WL
      AMO3L2=VO3LEE*VO3LEE/AW2L
      P6P3LE=(7.*AMO3L2-1)/6.
C     CALC. PLEE FIRST WITH STRAIGHT TRANS. WAVE ASSUMPTION
C     THEN CORRECT PLEE WITH RATIO PLEEO/PREF
      PLEE=P6P3LE*PWP1L*P1
      PLEE=PLEE*PLEEO/PREF
      P6P3LE=PLEE/(PWP1L*P1)
      AMO3L2=(6*P6P3LE+1.)/7.
      R6R3LE=6.*AMO3L2/(AMO3L2+5.)
      A6LEE2=AW2L*P6P3LE/R6R3LE
      AM6OL2=(AMO3L2+5.)/(7.*AMO3L2-1.)
```

```
      V60LEE=-SQRT(AM60L2)*SQRT(A6LEE2)
      VO3LEE=SQRT(AMO3L2)*SQRT(AW2L)
      VOWLEE=VO3LEE+V3WL
      V6WLEE=V60LEE+VOWLEE
      DLEE=(1000000*X/COS(TCR))*((VOWLEE-V6WLEE)/(V6WLEE*VOWLEE))
      IF(BOS.EQ.0) GO TO 202
      DURALE=-DLEE*BETA/BOS+DLEE
      GO TO 203
  202 DURALE=0
C     BETA GREATER THAN BOS
  203 U2W=(VB-V2BT)*COS(BETA)+V1*COS(AL)
      V2W=(VB-V2BT)*SIN(BETA)+V1*SIN(AL)
      ALE=ATAN(V2W/U2W)
      V2WT=(U2W*U2W+V2W*V2W)**.5
      AM2=V2WT/SQRT(A22)
      IF(BETA.LT.BOS) GO TO 36
      V2WT=(V2W*V2W+U2W*U2W)**.5
      AM2=V2WT/SQRT(A22)
      THETE=TCR-AL
      CPHI=SIN(TCR)*COS(ALE)-COS(TCR)*SIN(ALE)
      PC=.5*R2R1*R1*V2WT**2*CPHI*((2-.46/AM2)*CPHI+.46/AM2)/(144*32.2)
      PLEE=PA+PC
      P6P3LE=PLEE/(PWP1L*P1)
      AMO3L2=(6.*P6P3LE+1)/7.
      VO3LEE=SQRT(AMO3L2)*SQRT(AW2L)
      VOWLEE=VO3LEE+V3WL
      DURALE=0
   36 CONTINUE
      ENGTIM=(1000000.*X/COS(TCR))*(1./VOWLEE-1./VOWEFF)
      IF(BETA.EQ.0) ENGTIM=0
      WRITE(6,34)ENGTIM
   34 FORMAT(/6X,'ENGULFMENT TIME(MICRO-SEC)=',F8.2)
      WRITE(6,39)
   39 FORMAT(//6X,'CIRCUMFERENTIAL',10X,'PRE-ENCOUNTER',10X,'PEAK PRESSU
     *RE',11X,'QUASI-STEADY',9X,'PULSE DURATION'/7X,'ANGLE,PHI-DEG',12
     *X,'PRESSURE-PSI',15X,'PSI',16X,'PRESSURE-PSI',10X,'MICRO-SEC')
```

```
C     CIRCUMFERENTIAL DISTRIBUTION OF PRESSURE(PC) AND PULSE
C     QUANTITY(PHID)
      DO 5 IJ=1,10
      PHI=(IJ-1)*20/57.3
      PHID=PHI*57.3
      PHIX=PHI/2
      IF(BETA.EQ.0..AND.ALD.EQ.0) GO TO 9
      AK=VOWLEE/VOWEFF
      AK1=(1.+AK)/(1.-AK)
      AK2=(1.-AK1)*VOWEFF
C     VO=WAVE FRONT VELOCITY REL TO SURFACE
      VO=AK2/(COS(PHI)-AK1)
    9 IF(BETA.EQ.0..AND.ALD.EQ.0) VO=VOWEFF
      PWP1C=PWP1O
      RWR1C=RWR1O
      AW2C=A3W2
      V3WC=V3WWT
      IF(ALPHA.EQ.0) GO TO 10
C     ESTIMATE PRE-ENCOUNTER SURFACE PRESSURE,SND SPD AND VELOCITY
      PHIX=PHI/2
      PWP1C=PWP1W-(PWP1W-PWP1LE)*(SIN(PHIX))**2
      RWR1C=RWR1W-(RWR1W-RWR1LE)*(SIN(PHIX))**2
      AW2C=PWP1C*A1**2/RWR1C
      V3WC=VW+(V3WLEE-VW)*(SIN(PHIX))**2
      PI=PWP1C*P1
   10 CONTINUE
      V3=VO-V3WC
      AMO=V3*V3/AW2C
      P6P3=(7.*AMO-1.)/6
      PC=P6P3*PWP1C*P1
C     QUASI STEADY PRESSURE
      BK=COS(ALE)*SIN(TCR)
      CK=SIN(ALE)*COS(TCR)
      CGAM=BK+CK*COS(PHI)
      PD=PA
      PQS=PD+.5*R2R1*R1*V2WT**2*CGAM*((2.-.46/AM2)*CGAM+.46/AM2)/(
```

```
     *144*32.2)
C    PULSE DURATION
     DW=DWS
     DL=DURALE
     IF(REG.EQ.1)DW=DREG
     DURA=DW-(DW-DL)*(SIN(PHIX))**2
     R6R3=6.*AMO/(AMO+5.)
     A62=AW2C*P6P3/R6R3
     AM602C=(AMO+5.)/(7.*AMO-1.)
     V60C=-SQRT(AM602C)*SQRT(A62)
     V6WC=V60C+VO
     DC=(1000000*X/COS(TCR))*((VO-V6WC)/(VOWEFF*V6WC))
     POSPW=POS/(PWP1C*P1)
     AMOS=(6.*POSPW+1.)/7.
     V30S=SQRT(AMOS)*SQRT(AW2C)
     ROSRW=6.*AMOS/(AMOS+5.)
     VOSO=V30S+V3WC
     AOS2=AW2C*POSPW/ROSRW
     AMOS6=(AMOS+5.)/(7.*AMOS-1.)
     VOS6=-SQRT(AMOS6)*SQRT(AOS2)
     VOS6W=VOS6+VOSO
     T=1000000*X/(COS(TCR)*VOWEFF)
     DOS=(VOSO-VOS6W)*T/VOS6W
     D=(VO-VOS6W)*T/VOS6W
     IF(POS.GE.PC)D=0.
     WRITE(6,40)PHID,PI,PC,POS,DURA
  40 FORMAT(10X,F7.2,16X,F8.2,15X,F8.2,15X,F8.2,15X,F8.2)
   3 CONTINUE
 302 CONTINUE
 900 CONTINUE
 901 CONTINUE
     STOP
     END
```

5.0 CONCLUSIONS

The primary conclusion drawn from this study was that it is possible to formulate a reasonably accurate semi-empirical model of the shock-on-shock phenomenon. As with any such model the range of applicability, until it's demonstrated otherwise, is assumed to be limited to the range of parameters for which test data are available. However, the empiricism was kept to a level which should allow the model to be used effectively over a much larger range of conditions (i.e., blast strengths) than that covered by the existing data.

The model is cost effective in that a set of encounter angles can be examined with no more than a few seconds of CPU time on the IBM 370/158.

The model deals effectively with small angles of attack, but must become increasingly suspect as the angle of attack exceeds the cone half-angle. This caution is noted because very little test data are available for a cone at angle of attack in a blast environment to compare the accuracy of the prediction method, and because of the occurrence of flow separation on the leeside of the cone when the angle of attack exceeds the cone half-angle (approximately). The occurrence of separation is not accounted for in this model and, therefore, is a possible improvement that should be addressed as a future task.

REFERENCES

1. Kutler, P. and Sakell, L., 1"Three-Dimensional, Shock-on-Shock Interaction Problem," AIAA paper No. 75-49, San Diego, California, January 1975.

2. Reutenik, J. R., et al, Shock-on-Shock Measurements At Mach 3 and 5 From Rocket-Propelled Sled Tests, Phases 2 and 3: Oblique Intercepts, Defense Nuclear Agency Report DNA 3813F-1, Nov. 1975.

3. Aiello, G. F., Support of Phase II and III of the Shock-on-Shock Sled Test Program, Defense Nuclear Agency Report DNA 3787F, October 1975.

4. Inger, G. R., "Oblique Blast Impingement on Slender Hypersonic Bodies," AIAA Journal, Vol. R, No. 8, August 1966, pp 1475-1477.

5. McNamara, W., "FLAME Computer Code for the Axisymmetric Interaction of a Blast Wave with a Shock Layer on a Blunt Body," Journal of Spacecraft and Rockets, Vol 4, No. 6, June 1967, pp 790.

6. Taylor, T. D., "Shock-Shock Interaction Theory Including Real Gas and Three-Dimensional Effects," Aeroneutronic Research Laboratory, Prepared for Picatinny Arsenal, Technical Report No. 3319, April 1966.

7. Brown, E. A. and Mullaney, G. J., "Experiments on the Head-on Shock-Shock Interaction," AIAA Journal, Vol. 3, No. 11, November 1965, pp 2168-2170.

8. Merritt, D. L. and Aronson, R. M., "Wind Tunnel Simulation of Head-on Bow Wave-Blast Wave Interactions," Naval Ordnance Laboratory, NOLTR 67-123, August 1967.

9. Merritt, D. L. and Aronson, P. M., "Experimental Studies of Shock-Shock Interactions on a Nine Degree Cone," NOLTR 67-182, January 1968.

10. Baltakis, F. P., "Shock Interaction Surface Pressures for Hemispherical and Conical Bodies," NOLTR 71-27, February 1971.

11. Ames Research Staff, Equations, Tables, and Charts for Compressible Flow, NACA Report 1135, 1953.

12. Kutler, P., Letter to Martin Marietta from National Aeronautics and Space Administration, Ames Research Center, March 28, 1975.

13. The Martin Marietta Approach to Interceptor Missile Subsystem SPRINT, Vol. I Appendix, Martin Marietta Report OR 2900P, Feb. 1963 (Confidential).

14. Smyrl, J. L., The Impact of a Shock Wave on a Thin Two-Dimensional Airfoil Moving at Supersonic Speeds, Journal of Fluid Mechanics, Vol. 4, 1963.

DISTRIBUTION LIST

NAME	COPIES
DEPARTMENT OF DEFENSE	
Director Defense Advanced Rsch Proj Agency Architect Building 1400 Wilson Blvd. Arlington, VA 22209	
ATTN: Strategic Tech Office	1
Defense Documentation Center Cameron Station Alexandria, VA 22314	
ATTN: TC	12
Director Defense Intelligence Agency Washington, DC 20301	
ATTN: DT-7D	1
ATTN: DT-1C Nuc Eng Branch	1
ATTN: DT-2 WPNS & Sys Div	1
Director Defense Nuclear Agency Washington, DC 20305	
ATTN: STTL Tech Library	3
ATTN: STST Archives	1
ATTN: DDST	1
ATTN: SPAS	3
ATTN: STSP	1
Dir of Defense RSCH & Engineering Department of Defense Washington, DC 20301	
ATTN: DD/S&SS	1
ATTN: AD/OS	1
ATTNL AD/DS	1
Commander Field Command Defense Nuclear Agency Kirtland AFB, NM 87115	
ATTN: FCTMOF	1
ATNN: FCPR	1
ATTN: FCTMD	1

NAME	COPIES
Director	
Joint Strat Tgt Planning Staff JCS	
Offutt AFB	
Omaha, NB 68113	
ATTN: JLTW-2	1
ATTN: JPTM	1
ATTN: JPTP	1
Chief	
Livermore Division Fld Command DNA	
Lawrence Livermore Laboratory	
P.O. Box 808	
Livermore, CA 94550	
ATTN: FCPRL	1

DEPARTMENT OF ARMY

NAME	COPIES
Program Manager	
BMD Program Office	
1300 Wilson Blvd.	
Arlington, VA 22209	
ATTN: DACS-BMZ	1
ATTN: DACS-BMT John Shea	1
ATTN: DACS-BMZ-D Julian Davidson	1
ATTN: DACS-BMT Clifford E. McLain	1
Command	
BMD System Command	
P.O. Box 1500	
Huntsville, AL 35807	
ATTN: BDMSC-TEN Noah J. Hurst	1
Dep Chief of Staff for RSCH Dev & Acq	
Department of the Army	
Washington, DC 20310	
ATTN: NCB Division	1
Deputy Chief of Staff for OPS & Plans	
Department of the Army	
Washington, DC 20310	
ATTN: Dir of Chem & Nuc Ops	1
Commander	
Harry Diamond Laboratories	
2800 Powder Mill Road	
Adelphi, MD 20783	
ATTN: DRXDO-RC Robert B. Oswald, Jr.	1
ATTN: DRXDO-NP	1
ATTN: DRXDO-RBH James H. Gwaltney	1

NAME	COPIES
Commander Picatinny Arsenal Dover, NJ 07801	
ATTN: SMUPA-MD Henry Opat	1
ATTN: SARPA-ND-C-T Donald Miller	1
ATTN: SARPA-FR-E Louis Avrami	1
Commander Trasana White Sands Missile Range, NM 88002	
ATTN: R.E.Dekinder, Jr.	1
Director U.S. Army Ballistic Research Labs Aberdeen Proving Ground, MD 21005	
ATTN: Robert E. Eichelberger	1
ATTN: DRXBR-TB J.T. Frasier	1
ATTN: DRXRD-BVL William J. Schuman, Jr.	1
Commander U.S. Army Mat & Mechanics Rsch Ctr Watertown, MA 02172	
ATTN: DRXMR-HH John F. Dignam	1
Command U.S. Army Materiel Dev & Readiness Cmd 5001 Eisenhower Avenue Alexandria, VA 22333	
ATTN: DRCDE-D Lawrence Flynn	1
Commander U.S. Army Missile Command Redstone Arsenal, AL 35809	
ATTN: DRSMI-XS Chief Scientist	1
ATTN: DRSMI-RRR Bud Gibson	1
ATTN: DRS-RKP W.B. Thomas	1
ATTN: DRCPM-PE-EA Wallace O. Wagner	1
Commander U.S. Army Nuclear Agency Fort Bliss, TX 79916	
ATTN: ATCA-NAW	1
DEPARTMENT OF NAVY	
Chief of Naval Material Navy Department Washington, DC 20360	
ATTN: Mat 0323 Irving Jaffe	1

NAME	COPIES
Chief of Naval Research	
Navy Department	
Arlington, VA 22217	
ATTN: Code 464 Thomas P. Quinn	1
Director	
Naval Research Laboratory	
Washington, DC 20375	
ATTN: Gerald Copperstein Code 7770	1
ATTN: Code 5180 Mario A. Persechino	1
ATTN: Code 2027 Tech Lib	1
Commander	
Naval Sea Systems Command	
Navy Department	
Washington, DC 20362	
ATTN: 0333A Marlin A. Kinna	1
Commander	
Naval Surface Weapons Center	
White Oak, Silver Spring, MD 20910	
ATTN: Code 323 W. Carson Lyons	1
ATTN: Code WA501 Navy Nuc Prgms Off	1
ATTN: Code 2302 Leo F. Gowen	1
Director	
Strategic Systems Project Office	
Navy Department	
Washington, DC 20376	
ATTN: NSP-272 CDR Leslie Stoessl	1

DEPARTMENT OF THE AIR FORCE

AF Materials Laboratory, AFSC	
Wright-Patterson AFB, OH 45433	
ATTN: MAS	1
ATTN: MBC Donald L. Schmidt	1
ATTN: T. Nicholas	1
AF Rocket Propulsion Laboratory, AFSC	
Edwards AFB, CA 93523	
ATTN: RTSN G.A. Beale	1
AF Weapons Laboratory, AFSC	
Kirtland AFB, NM 87117	
ATTN: SUL	1
ATTN: DYS Lt. F.J. Burns	1
ATTN: DYV	1
ATTN: Dr. Minge	1

NAME	COPIES
Commander	
Foreign Technology Division, AFSC	
Wright-Patterson AFB, OH 45433	
ATTN: TDFRD J. D. Pumphrey	1
ATTN: TDPTN	1
Hq USAF/RD	
Washington, DC 20330	
ATTN: RD	1
SAMSO/MN	
Norton AFB, CA 92409	
(Minuteman)	
ATTN: MNNR	1
SAMSO/RS	
Post Office Box 92960	
Worldway Postal Center	
Los Angeles, CA 90009	
(Reentry Systems)	
ATTN: RSSF	1
ATTN: RSS	1
Command in Chief	
Strategic Air Command	
Offutt AFB, NB 68113	
ATTN: DOXT	1
ATTN: XPFS	1

U.S. ENERGY RESEARCH AND DEVELOPMENT ADMINISTRATION

Division of Military Application	
U.S. Energy Rsch & Dev Admin	
Washington, DC 20545	
ATTN: Doc Con for Res & Dev Branch	1
ATTN: Doc Con for CDR Richard E. Peterson	1
ATTN: Doc Con for LTC Donald L. McNutt	1
University of California	
Lawrence Livermore Laboratory	
P.O. Box 808	
Livermore CA 94550	
ATTN: C. Joseph Taylor L-92	1
ATTN: Joseph E. Keller, Jr. L-125	1
ATTN: G. Staihle L-24	1

NAME	COPIES
Los Alamos Scientific Laboratory P.O. Box 1663 Los Alamos, NM 87545	
ATTN: Doc Con for J.W. Taylor	1
ATTN: Doc Control for John McQueen	1
ATTN: Doc Control for R.S. Thurston	1
Sandia Laboratories Livermore Laboratory P.O. Box 969 Livermore, CA 94550	
ATTN: Raymond NG	1
ATTN: Doc Control for T. Gold	1
ATTN: Doc Control for C.S. Hoyle	1
ATTN: Doc Con for 8131 H.F. Norris, Jr.	1
Sandia Laboratories P.O. Box 5800 Albuquerque, NM 87115	
ATTN: Doc Con for Albert Chabai	1
ATTN: Doc Con for R.R. Boade	1
ATTN: Doc Control for D. McCloskey	1

DEPARTMENT OF DEFENSE CONTRACTORS

NAME	COPIES
Aeronautical Rsch Assoc of Princeton Inc. 50 Washington Road Princeton, NJ 08540	
ATTN: Coleman Donaldson	1
Aeronutronic Ford Corporation Aerospace & Communications Ops Aeronutronic Division Ford & Jamboree Roads Newport Beach, CA 92663	
ATTN: P. Spangler	1
Aerospace Corporation P.O. Box 92957 Los Angeles, CA 90009	
ATTN: W. Barry	1
ATTN: R. Allen	1
ATTN: Richard Crolius A2-RM1027	1
AVCO Research & Systems Group 201 Lowell Street Wilmington, MA 01887	
ATTN: John Gilmore E502	1
ATTN: John E. Stevens E500	1

NAME	COPIES
Battelle Memorial Institute 505 King Avenue Columbus, OH 43201	
ATTN: Merwyn R. Vanderlind	1
ATTN: W. Pfeifer	1
Boeing Company, The P.O. Box 3707 Seattle, WA 98124	
ATTN: Brian Lempriere	1
Brown Engineering Company, Inc. Cummings Research Park Huntsville, AL 35807	
ATTN: Ronald Patrick	1
Effects Technology, Inc. 5383 Hollister Avenue Santa Barbara, CA 93111	
ATTN: Robert Wengler	1
General Electric Company Space Division Valley Forge Space Center Goddard Blvd King of Prussia P.O. Box 8555 Philadelphia, PA 19101	
ATTN: G. Harrison	1
ATTN: Carl Anderson	1
ATTN: Philip Cline Rm 3700	1
General Electric Company Tempo-Center for Advanced Studies 816 State Street (P.O. Drawer QQ) Santa Barbara, CA 93102	
ATTN: DASTAC	1
Institute for Defense Analysis 400 Army-Navy Drive Arlington, VA 22202	
ATTN: Joel Bengston	1
ATTN: Ida Librarian Ruth S. Smith	1
Kaman Avidyne Division of Kaman Sciences Corp 83 Second Avenue Northwest Industrial Park Burlington, MA 01803	
ATTN: Norman P. Hobbs	1

NAME	COPIES
Kaman Sciences Corporation P.O. Box 7463 Colorado Springs, CO 80933	
ATTN: Albert P. Bridges	1
ATTN: Thomas Meagher	1
ATTN: Frank H. Shelton	1
ATTN: Jerry L. Harper	1
ATTN: John R. Hoffman	1
Lockheed Missiles and Space Company 3251 Hanover Street Palo Alto, CA 94304	
ATTN: A.P. Hardt	1
ATTN: Lloyd F. Chase	1
ATTN: Raymond R. Capiaux	1
ATTN: F.G. Borgardt	1
Martin Marietta Aerospace Orlando Division P.O. Box 5837 Orlando, FL 32805	
ATTN: Laird Kinnaird	1
McDonnell Douglas Corporation 5301 Bolsa Avenue Huntington Beach, CA 92647	
ATTN: L. Cohen	1
ATTN: J. Kirby	1
ATTN: J.F. Garibotti	1
ATTN: R.J. Reck	1
Physics International Company 2700 Merced Street San Leandro, CA 94577	
ATTN: Doc Con for James Shea	1
Prototype Development Associates Inc. 1740 Garry Avenue Santa Ana, CA 92705	
ATTN: John Slaughter	1
R&D Associates P.O. Box 9695 Marina Del Rey, CA 90291	
ATTN: Albert L. Latter	1
ATTN: Jerry Carpenter	1
ATTN: Harold L. Brode	1
ATTN: F.A. Field	1

NAME	COPIES
Science Applications, Inc. P.O. Box 2351 La Jolla, CA 92038	
ATTN: R. Fisher	1
ATTN: G. Ray	1
Science Applications, Inc. 101 Continental Blvd. Fl Segundo, CA 90245	
ATTN: J. Courtney	1
Southern Research Institute 2000 Ninth Avenue South Birmingham, AL 35205	
ATTN: C.D. Pears	1
Stanford Research Institute 333 Ravenswood Avenue Monlo Park, CA 94025	
ATTN: Donald Curran	1
ATTN: Herbert E. Lindberg	1
ATTN: George R. Abrahamson	1
Stanford Research Institute 306 Wynn Drive, N.W. Huntsville, AL 35805	
ATTN: Harold Carey	1